Neurobiology of Disease 132 (2019) 104529

Contents lists available at ScienceDirect

Neurobiology of Disease

journal homepage: www.elsevier.com/locate/ynbdi

Perturbed Ca^{2+}-dependent signaling of DYT2 hippocalcin mutant as mechanism of autosomal recessive dystonia

D.S. Osypenko[a,d,1], A.V. Dovgan[a,1], N.I. Kononenko[a], A.V. Dromaretsky[a], M. Matvieienko[a], O.A. Rybachuk[c], J. Zhang[b], S.M. Korogod[a], V. Venkataraman[b], P. Belan[a,d,*]

[a] Departments of Molecular Biophysics, Bogomoletz Institute of Physiology, Kyiv, Ukraine
[b] Rowan University, Stratford, NJ, USA
[c] Sensory Signaling, Bogomoletz Institute of Physiology, Kyiv, Ukraine
[d] Kyiv Academic University, Ukraine

ARTICLE INFO

Keywords:
Primary dystonia
Hippocalcin
Dystonia-causing mutations
Slow afterhyperpolarization

ABSTRACT

A recent report of autosomal-recessive primary isolated dystonia (DYT2 dystonia) identified mutations in *HPCA*, a gene encoding a neuronal calcium sensor protein, hippocalcin (HPCA), as the cause of this disease. However, how mutant HPCA leads to neuronal dysfunction remains unknown. Using a multidisciplinary approach, we demonstrated the failure of dystonic N75K HPCA mutant to decode short bursts of action potentials and theta rhythms in hippocampal neurons by its Ca^{2+}-dependent translocation to the plasma membrane. This translocation suppresses neuronal activity via slow afterhyperpolarization (sAHP) and we found that the N75K mutant could not control sAHP during physiologically relevant neuronal activation. Simulations based on the obtained experimental results directly demonstrated an increased excitability in neurons expressing N75K mutant instead of wild type (WT) HPCA. In conclusion, our study identifies sAHP as a downstream cellular target perturbed by N75K mutation in DYT2 dystonia, demonstrates its impact on neuronal excitability, and suggests a potential therapeutic strategy to efficiently treat DYT2.

1. Introduction

Primary dystonia is a neurological movement disorder syndrome in which sustained or repetitive muscle contractions result in twisting and repetitive movements or abnormal painful postures. The brain of patients with primary dystonia contains no overt abnormalities (Tanabe et al., 2009). At the same time, anatomical and functional imaging demonstrates different abnormalities in many brain regions including the cerebral cortex, striatum, cerebellum, thalamus, midbrain/brainstem as well as the hippocampus that may contribute to manifestation of dystonia symptoms (Bostan and Strick, 2012; Ceballos-Baumann et al., 1995; Ceballos-Baumann and Brooks, 1997; Edwards et al., 2003; Smit et al., 2018). Thus, dystonia is not driven by the activity of a single brain nucleus, but, rather, might arise from a broadly dysfunctional motor system (Balint et al., 2018; Tanabe et al., 2009) indicating to changes in functioning of widely expressed gene(s).

Importantly, patients with both idiopathic and functional dystonia demonstrated differences in the volume of gray matter in the hippocampus (Piccinin et al., 2015; Tomic et al., 2018). Moreover, in combined dystonia, a tight relationship is shown between morphological and functional abnormalities in the hippocampus and symptoms of dystonia (Kuba et al., 2010; Rasouli et al., 2018). Furthermore, important changes in synaptic drive (Kakazu et al., 2012; Yokoi et al., 2015), regulation of Ca^{2+} concentration (Iwabuchi et al., 2013) and expression of Ca^{2+} binding proteins (Byun et al., 2013) were observed in the hippocampus in different animal models of dystonia. Altogether, these recent findings imply that the hippocampal abnormalities are likely to be directly associated with dystonic symptoms and that the hippocampus seems to be involved in the network underlying the disease.

The recent genetic study of patients with DYT2 dystonia revealed three point mutations in *HPCA*, a gene encoding a neuronal calcium sensor (NCS) protein, hippocalcin (HPCA). The gene is almost exclusively expressed in the brain with high level of expression in the cortex, striatum, cerebellum and hippocampus (Charlesworth et al., 2015), i.e. in brain areas revealing abnormalities in dystonia (Balint et al., 2018; Tanabe et al., 2009). HPCA contains three EF-hand domains capable of binding Ca^{2+} (Helassa et al., 2017; O'Callaghan et al.,

* Corresponding author at: Departments of Molecular Biophysics, Bogomoletz Institute of Physiology, Kyiv, Ukraine.
E-mail address: pasha@biph.kiev.ua (P. Belan).
[1] These authors equally contributed to this work.

https://doi.org/10.1016/j.nbd.2019.104529
Received 4 April 2019; Received in revised form 22 June 2019; Accepted 9 July 2019
Available online 10 July 2019
0969-9961/

2003). The binding results in a Ca^{2+}-myristoyl switch, a Ca^{2+}-dependent conformation change leading to protrusion of its myristoyl-containing N-terminal region out of a hydrophobic pocket of the molecule (Ames et al., 1997). This allows HPCA to translocate from the cytosol to the plasma membrane (Dovgan et al., 2010; Kobayashi et al., 1993; Markova et al., 2008; O'Callaghan et al., 2003). It is established that this Ca^{2+}-dependent translocation of HPCA leads to inhibition of cortical and hippocampal neurons by gating a slow afterhyperpolarization (sAHP) current (Andrade et al., 2012; Kim et al., 2012; Tzingounis et al., 2007; Villalobos and Andrade, 2010). HPCA mutations at positions T71N and N75K shown in development of DYT2 dystonia are within its second EF-hand domain that may impair its Ca^{2+} binding properties (Charlesworth et al., 2015), prevent HPCA translocation and decrease the neuronal inhibition. Importantly, functional imaging and PET indicate that dystonia is associated with impaired inhibition in both cortical and subcortical regions (Ibanez et al., 1999; Levy and Hallett, 2002). Thus, we have hypothesized that the DYT2 mutations perturb HPCA signaling and sAHP gating leading to increased neuronal excitability. We tested this hypothesis using hippocampal neurons, which potentially belong to disease-causing network (Kuba et al., 2010; Rasouli et al., 2018) and are the most studied cellular model of HPCA-dependent gating of sAHP (Andrade et al., 2012; Tzingounis et al., 2007).

In this work, we initially tested effects of the dystonia-causing mutations on the biophysical properties of HPCA and found that N75K mutant (rather than T71N) had lower Ca^{2+} buffer capacity and decreased Ca^{2+}-sensitivity compared to wild type (WT) HPCA. This mutant also revealed strong deficiency in Ca^{2+}-dependent translocation to the plasma membrane of hippocampal neurons leading to impaired sAHP gating. A model of HPCA and N75K mutant signaling in a cortical neuron demonstrated a dramatic increase in the cellular excitability in different experimental settings. We have concluded that N75K mutation may cause DYT2 dystonia via impaired regulation of slow afterhyperpolarization.

2. Materials and methods

2.1. HEK 293 cell culture

Undifferentiated HEK 293 (HEK) cells were obtained from the Cell Culture Bank of National Academy of Sciences of Ukraine (Bogomoletz Institute of Physiology, Kiev, Ukraine). The HEK cells were cultured on round glass coverslips in DMEM supplemented with 10% fetal bovine serum and 0,25% gentamycin. The cells were maintained in 12-well culture dishes at 37 °C, in a 5% CO_2 humidified atmosphere. The culture medium was changed every 3–5 days and cells were split when necessary. Cells were transfected at ~75% confluence with 0.3–0.5 μg of DNA per well using Lipofectamine 3000 (Thermo Scientific, USA) and then cultured for 1–3 days until they were used in experiments.

2.2. Hippocampal cultures

All procedures used in this study were approved by the Animal Care Committee of Bogomoletz Institute of Physiology and conform to the Guidelines of the National Institutes of Health on the Care and Use of Animals. Neurons were obtained from newborn Wistar rats (age postnatal day 0–1; 56 animals of both sexes for the whole work) killed via rapid decapitation without anaesthesia. All rats were from the vivarium of Bogomoletz Institute of Physiology. Hippocampi of the rats were enzymatically dissociated with trypsin. The cell suspension (initial density of $3–5 \times 10^5$ cells per cm^3) was plated on glass coverslips coated with laminin and poly-L-ornithine (Thermo Fisher Scientific, USA). Cells were maintained in feeding solution consisting of minimal essential medium, 1% horse serum 1% N2 supplement and 2% of B27 supplement (Thermo Fisher Scientific, USA) in a humidified atmosphere containing 5% CO_2 at 37 °C as previously described (Dovgan et al., 2010).

2.3. Plasmids

HPCA-YFP, HPCA-CFP, HPCA and enhanced yellow and cyan fluorescent protein (YFP, CFP) plasmids were prepared as described previously (O'Callaghan et al., 2002).

To create the dystonia-associated mutations, T71N and N75K, the following primers were used: T71N: Fwd CAT GTC TTC CGC AAT TTT GAC ACC AAC -3′, Rev. 5′- GTT GGT GTC AAA ATT GCG GAA GAC ATG -3′. N75K: Fwd 5′- ACT TTT GAC ACC AAA GCG ACG GCA CCA -3′, Rev5′- TGG TGC CGT CGC TTT GGT GTC AAA AGT -3′. Mutations were created using the QuikChange II XL Site-Directed Mutagenesis kit from Agilent Technologies (Santa Clara, CA, USA) using standard protocols. All constructs were confirmed via sequencing.

2.4. Transient transfection

Hippocampal neurons were transfected after 13–17 days in culture using Lipofectamine 2000 transfection reagent essentially as described by the supplier (Thermo Fisher Scientific, USA). All cultures were used for the experiments 2–3 days after transfection.

2.5. Electrophysiological recordings

Neurons growing in the cultures were visualized using inverted microscopes (IX70 or IX71; Olympus, Japan). Whole-cell patch-clamp recordings in either current- or voltage-clamp mode were obtained using an EPC-10/2 amplifier controlled by PatchMaster software (HEKA, Germany). The composition of the extracellular solution was as follows (mM): NaCl 150, KCl 2.5, $CaCl_2$ 2, $MgCl_2$ 1, HEPES 10, glucose 10, pH 7.3, osmolarity 325–330 mOsm. sAHP recordings were carried out in the presence of ionotropic glutamate receptor blockers, D-2-amino-5-phosphonopentanoic acid (APV, 40 μM) and 6-cyano-7-nitroquinoxaline-2,3-dione (CNQX, 10 μM). Gabazine (5 μM) was always present in the extracellular solution to block $GABA_A$ receptors. The intracellular solution contained (mM): K-Methansulfonate 135, KCl 10, EGTA 0.2, MgATP 4, Na-GTP 0.4, Na_2-Phosphocreatin 5, HEPES 10, pH 7.3, osmolarity 300–305 mOsm. In translocation experiments conducted in a voltage clamp mode, K^+ was replaced with Cs^+ and 3–5 mM QX-314, an intracellular sodium channel blocker, was added. The transfected neurons were patched in the whole cell configuration and translocation was induced by depolarization from −70 to 0 mV of varying durations from 0.125 s up to 4.0 s. Patch electrodes were pulled to obtain a resistance of 2–4 MΩ. Membrane voltage or transmembrane current were low-pass filtered (3 kHz) and acquired at 20 kHz. Recordings with a leak current > 200 pA or a series resistance of > 30 MΩ were discarded. All experiments were conducted at room temperature.

2.6. Fluorescence measurements of protein translocation

Time-lapse imaging of HEK cells and hippocampal neurons transiently transfected with fluorescent protein(s) was performed using a TILL Photonics wide-field imaging system (TILL Photonics, Germany) installed on inverted microscopes (IX70 or IX71, Olympus, Japan), using oil immersion objectives (×40, NA 1.35 or ×60, NA 1.25; Olympus, Japan), controlled by TILLvision or LA software (TILL Photonics, Germany). An Imago CCD camera was used to record changes in fluorescence, with acquisition rate typically in the range 0.5–2 Hz. Customized routines written in TILLvision software and MatLab (MathWorks, USA) were used to calculate relative changes in fluorescence against initial baseline level in order to reveal sites of protein translocation. A value of translocation, $\Delta F/F_0$, was expressed as relative changes in fluorescence of fluorescent protein tagged to a protein under study; F_0 is an initial value of fluorescence (before

electrical stimulations or uncaging) while ΔF is a difference between a current and initial values.

The following routine was used to determine translocation sites, over which regions of interest (ROIs) were placed and averaged values of HPCA-FP fluorescence were calculated to demonstrate spatio-temporal patterns of HPCA translocation. Base and shifted movies were generated based on an initial movie recorded during imaging experiments. Each frame of the base movie was generated by averaging two to five frames of the initial movie, each frame of the shifted movie was generated by averaging the same number of frames (two to five) of the initial movie with a two- to seven-frame shift between base and shifted movies. The particular number of frames for averaging and shifting depended on the kinetics of protein translocation transients and acquisition frame rate. The base movie was subtracted from the shifted movie. An averaging filter with 3 × 3 kernel spatially filtered the differential movie. Translocation sites were determined as simply connected regions with a level of HPCA-FP fluorescence at least 2% higher than the baseline fluorescence. A green colour in all images represents a decrease and red one represents an increase in HPCA-FP fluorescence. Photobleaching was compensated as previously described (Dovgan et al., 2010).

Decay kinetics of translocation transient was calculated as weighted τ by means of dividing an area under the transient by its amplitudes.

In order to observe HPCA-FP translocation without substantial disturbance of intrinsic regulation of intracellular free calcium concentration ($[Ca^{2+}]_i$), we mainly studied translocation during the first 10–15 min after establishing a patch clamp configuration and/or in distal parts of a dendritic tree (100–350 µm from soma).

2.7. Ca^{2+}-uncaging and imaging in HEK cells

HEK cells were loaded with a Ca^{2+} dye Fura Red AM and 'caged' Ca^{2+} substance NP-EGTA AM (5 µM each, Thermo Fisher Scientific, USA). To ensure the same loading rate in every experiment, cells were held at 37 °C for 30 min during loading. After that, an extracellular solution containing AM forms of Fura Red and NP-EGTA was replaced with a fresh extracellular solution. Intracellular $[Ca^{2+}]_i$ was increased by several consequent flashes of UV light (500–1000 ms @ 335 nm at 0.1 Hz) using a monochromator of TILL Photonics imaging system. $[Ca^{2+}]_i$ was simultaneously measured with the same frame rate as protein translocation (0.5–2.0 Hz) by means of Fura Red. Since Fura Red decreases its fluorescence when $[Ca^{2+}]_i$ increases, changes in $[Ca^{2+}]_i$ were shown as:

$$(F_0 - F)/F \text{ or } \Delta F/F$$

where F_0 is a fluorescence value right before uncaging and F is a current value of fluorescence. With such representation an increase in $[Ca^{2+}]_i$ led to an increase in $\Delta F/F$. These increases are linearly related only at $\Delta F << F_0$. Thus, $\Delta F/F$ represented a relative and nonlinear measure of $[Ca^{2+}]_i$. However, co-transfected HPCA and its mutant were subjected to identical spatio-temporal patterns of $[Ca^{2+}]_i$ in each HEK cell after uncaging (Fig. 2). Thus, $[Ca^{2+}]_i$-dependency of proteins' translocation could be obtained as a function of $\Delta F/F$ and compared for each cell (Figs. 2F, G, I, J).

The number and timing of subsequent flashes was chosen to substantially increase $[Ca^{2+}]_i$ and to simultaneously produce almost complete NP-EGTA uncaging at the end of the uncaging protocol. In this case, NP-EGTA itself did not substantially contribute to the total Ca^{2+} buffer capacity during the decay of $[Ca^{2+}]_i$ transient induced by the UV flashes. The flashes were repeated until no further increase in $[Ca^{2+}]_i$ was observable in HEK cells heterologously expressing HPCA or its mutants. Absence of the further decrease of Fura Red fluorescence, reflecting an increase in $[Ca^{2+}]_i$, was due to depletion of NP-EGTA rather than Fura Red saturation since amplitudes of $[Ca^{2+}]_i$ transients induced by the same set of flashes in neighboring nontransfected cells were significantly higher (Fig. 1A).

Not < 3 different culture preparations were employed for each type of experiment.

2.8. Comparisons of Ca^{2+} buffer capacities

The Ca^{2+} buffer capacity of Ca^{2+} buffer X, K_X, at a given $[Ca^{2+}]_i$ is defined as a ratio of buffer bound calcium concentration, Δ[XCa], necessary to increase a free calcium concentration by $\Delta[Ca^{2+}]_i$: $K_X = \Delta[XCa]/\Delta[Ca^{2+}]_i$ (Neher and Augustine, 1992).

Assuming that NP-EGTA and Fura Red loading is not dependent on expression of particular exogenous protein, any differences in the $[Ca^{2+}]_i$ transients between HPCA and its mutants will be due to a difference in their Ca^{2+} buffer capacity. Amplitude, A, and decay, τ, of the $[Ca^{2+}]_i$ transients can then be related to the Ca^{2+} buffer capacity of the exogenous buffer (e.g. WT HPCA, K_{WT}) by the following equations (Foehring et al., 2009; Helmchen et al., 1996):

$$A = \Delta[Ca^{2+}]_T/(1 + K_T + K_{WT})$$

$$\tau = (1 + K_T + K_{WT})/\gamma$$

where $\Delta[Ca^{2+}]_T$ is the increase in total Ca^{2+} (free and bound) due to the release from NP-EGTA upon its photocleavage, K_T is a sum of endogenous, NP-EGTA and Fura Red Ca^{2+} buffer capacities and γ is the Ca^{2+} extrusion rate. Thus, the amplitude of the $[Ca^{2+}]_i$ transients, A, is inversely dependent on K_{WT} while its decay, τ, depends linearly on K_{WT}.

In this work, the difference in decay kinetics of $[Ca^{2+}]_i$ transients was used to validate the difference in cytosolic Ca^{2+} buffer capacities. Although both A and τ can be used for such quantitative comparisons, the amplitudes of $[Ca^{2+}]_i$ transients, which were presented as relative changes in Fura Red fluorescence, $(F_0\text{-}F)/F$ (Figs. 1, 2), were subjected to a large systematic and poorly estimated error due to substantial crosstalk between Fura Red and CFP/YFP fluorescence channels. This crosstalk led to substantial contribution of fluorescent protein fluorescence to F_0 value in the Fura Red channel. In cells with high levels of expression of proteins under study, tagged by CFP or YFP, the crosstalk from fluorescent proteins could account for up to 70–80% of F_0 value in Fura Red channel. This crosstalk could not be precisely subtracted by linear unmixing resulting in non-estimated errors in F_0 values. In order to increase contribution of exogenously expressed proteins to Ca^{2+} buffer capacities we intentionally choose cells with high levels of protein expression thus far increasing the above error. Thus, although amplitudes of $[Ca^{2+}]_i$ transients were significantly higher in non-transfected compared HPCA-CFP transfected HEK cells (e.g. Fig. 1A) indicating to a lower buffer capacity of NT cells compared to the cells expressing HPCA-CFP, we decided not to use the amplitudes for statistical comparisons in this type of experiments.

The decay kinetics of $[Ca^{2+}]_i$ transients is not dependent on F_0 values and, therefore, could be used for comparisons of Ca^{2+} buffer capacities. At the same time, fluorescent protein translocation and their photobleaching could produce some errors in ΔF values in Fura Red channel. In order to cancel (or minimize) these errors, values of Fura Red fluorescence over the time course of $[Ca^{2+}]_i$ transients were divided by values of fluorescence of respective fluorescent protein recorded from the total area of the same HEK cell.

2.9. Statistics

Quantitative results are presented as mean ± SEM, and statistical significance between groups was tested using Student's *t*-tests, with equal variances and a confidence level of 0.05. The mean for each experiment was calculated as the average for all neurons tested with a given protocol.

2.10. Chemicals

Glutamate and $GABA_A$ receptor antagonists were obtained from

Table 1
Parameters for simulation of HPCA dynamics.

	HPCA	HPCA-Ca	HPCA-2Ca	HPCA_membr	HPCA_mutant	HPCA_mutant-Ca	HPCA_mutant-2Ca	HPCA_mutant_ membr	Buffer	Ca
Initial concentration (mM)	0.03821				0.03821				20	
Diffusion coefficient $D\left(\frac{\mu m^2}{ms}\right)$	0.05	0.05	0.05	0.001	0.05	0.05	0.05	0.001	0.05	0.22
$k_{f1}\left(\frac{1}{mM \cdot ms}\right)$	40	40			12	9			10	
$k_{b1}\left(\frac{1}{ms}\right)$	0.01	0.01			0.01	0.01			1	
$k_{f2}\left(\frac{1}{mM \cdot ms}\right)$			0.01				0.07			
$k_{b2}\left(\frac{1}{ms}\right)$			0.002				0.003			

Tocris (UK). All other chemicals were purchased from Sigma (USA) and Thermo Fisher Scientific (USA).

2.11. Computer simulation

Simulations were performed on a model of *neocortical layer 5 pyramidal neuron* developed in the NEURON program environment (Hines and Carnevale, 2001). It was our modification of the model described by Mainen and Sejnowski (Mainen and Sejnowski, 1996) and available from the open-access database ModelDB (access No. 2488) (Hines et al., 2004; Migliore et al., 2003). From the reference model we took the cell geometry (the reconstructed dendritic arborization, soma, and myelinated axon), mechanisms of intracellular calcium dynamics, biophysical properties and distribution of the ion channels. Particularly, the membrane of soma and axon contained voltage-dependent channels of fast-inactivating Na^+ and non-inactivating K^+ currents. The channels present in the dendritic membrane conducted the following currents: fast-inactivating Na^+, high voltage-activated non-inactivating Ca^{2+} (L-type), muscarinic K^+ (M-type); Ca^{2+}-dependent K^+ (SK-type) and passive leak (Mainen and Sejnowski, 1996). Our modifications of the reference model dendritic mechanisms were as follows: (1) Voltage-independent conductance *Gs* associated with the reversal potential *Es* = 0 mV was added to reproduce activation of excitatory postsynaptic receptors. (2) Kinetic properties of L-type Ca^{2+} current were modified to provide experimentally grounded time courses of Ca^{2+} entry and concentration profile. These properties were like in the model described by Papoutsi and co-authors (Papoutsi et al., 2017). (3) T-type Ca^{2+} current was added as its presence was shown in our experiments. This current properties were similar to those described by Vitko and co-authors (Vitko et al., 2005). (4) HPCA dynamics of both WT and mutant forms was added. The dynamics was represented by our original model (see below) describing HPCA binding to Ca^{2+}, insertion Ca^{2+}-bound HPCA into the membrane and its following unbinding and return to the cytosol. (5) Fast binding Ca^{2+} buffer was added to provide an explicit contribution to the dynamics of Ca^{2+} interacting with HPCA. (6) K^+ conductance dependent on the membrane fraction of HPCA simulating sAHP current was added. Like in the reference model, the modified conductances and mechanisms (1–3) were homogeneously distributed over the dendrites. Whereas other mechanisms (4–6) were present in particular dendritic sections (close to soma) to reflect a punctate dendritic distribution of HPCA translocation sites reported in our experiments (Dovgan et al., 2010; Markova et al., 2008).

The equations describing the ion currents and Ca^{2+} concentration inherited from the reference model can be found in the corresponding article (Mainen and Sejnowski, 1996). The modified model currents per unit membrane area were described by the following equations:

L-type calcium current (Papoutsi et al., 2017); ModelDB accession No. 230811):

$$J_{CaL} = G_{CaL} \cdot (m^2\, h + s^2) \cdot (V - E_{Ca}),$$

where V is the membrane potential; $G_{CaL} = 0.1$ mS/cm^2 and $E_{Ca} = 120$ mV are, respectively, maximum conductivity and reversal potential of the current; m, h, and s are kinetic variables of, respectively, voltage-dependent activation, Ca^{2+}-dependent inactivation, and activation, which obey the following equations:

$$dm/dt = (m_\infty - m)/\tau_m;\ m_\infty = 1/(1 + \exp(-(V - V_{1/2})/k))$$

$$k = 4.6 \cdot F/RT;\ \tau_m = 1.5 \text{ ms}$$

$$ds/dt = (s_\infty - s)/\tau_s;\ s_\infty = a/(a + 1)$$

$$a = ([Ca^{2+}]_i/0.03)^2;\ \tau_s = \tau_{min} + 1/([Ca^{2+}]_i + 0.01);\ \tau_{min} = 180 \text{ ms}$$

$$h = K/(K + [Ca^{2+}]_i);\ K = 0.025 \text{ mM}$$

F, R, and T are, respectively, Faraday constant, gas constant, and absolute temperature.

T-type calcium current (Vitko et al., 2005); ModelDB accession No. 53965):

$$J_{CaT} = G_{CaT} \cdot m^2 \cdot h \cdot (V - E_{Ca})$$

where $G_{CaT} = 0.1$ mS/cm^2 is maximum conductivity; m and h are, respectively, kinetic variables of voltage-dependent activation and inactivation obeying the following equations:

$$dm/dt = (m_\infty - m)/\tau_m;\ \tau_m = \tau_{min} + 1/(Q_{10} \cdot (\alpha_m + \beta_m))$$

$$\tau_{min} = 1.44 \text{ ms};\ m_\infty = \alpha_m \cdot \tau_m$$

$$\alpha_m = \exp((V + 51)/5.67);\ \beta_m = \exp(-(V + 128)/15.33)$$

$$dh/dt = (h_\infty - h)/\tau_h;\ \tau_h = \tau_{min} + 1/(Q_{10} \cdot (\alpha_h + \beta_h))$$

$$\tau_{min} = 26.67 \text{ ms};\ h_\infty = \alpha_h \cdot \tau_h$$

$$\alpha_h = \exp((V + 41)/4.32);\ \beta_h = \exp(-(V + 423.33)/53.33)$$

The HPCA dynamics was described by the following reaction-diffusion equations. The binding-unbinding reactions and transitions between cytosol and membrane fractions of both WT and mutant HPCA were described by the kinetic equations as follows.

Ca^{2+}-binding to free WT HPCA to form a "one Ca^{2+}-bound" cytosolic fraction, HPCA-Ca:

$$\text{HPCA} + Ca \underset{k_{b1}}{\overset{k_{f1}}{\rightleftarrows}} \text{HPCA-Ca}$$

Ca^{2+} binding to HPCA-Ca to form a "two Ca^{2+}-bound" cytosolic fraction.

$$\text{HPCA-Ca} + \text{Ca} \underset{k_{b1}}{\overset{k_{f1}}{\rightleftarrows}} \text{HPCA-2Ca}$$

Translocation of HPCA-2Ca from the cytosol to the plasma membrane to form a membrane HPCA-2Ca fraction, $HPCA_{membr}$, upon Ca^{2+}-myristoyl switch:

$$\text{HPCA-2Ca} \underset{k_{b2}}{\overset{k_{f2}}{\rightleftarrows}} \text{HPCA}_{\text{membr}}$$

Similar equations described the dynamics of the HPCA mutants, HPCAmut.

All reagents, including different forms of HPCA, buffer, and Ca^{2+} could freely diffuse both radially and longitudinally. For that, the intradendritic space was divided into discrete concentric cylindrical shells each subdivided into equally spaced longitudinal segments, so that changes in the intra-shell concentrations were described as.

$$\frac{\partial[Ca^{2+}]}{\partial t} = \Delta[Ca^{2+}]\cdot D_{Ca}\cdot\frac{S}{\Delta r}$$

$$\frac{\partial[Buffer]}{\partial t} = \Delta[Buffer]\cdot D_{Buffer}\cdot\frac{S}{\Delta r}$$

where D_{Ca} and D_{Buffer} are the diffusion coefficients of Ca^{2+} and buffer, respectively; S is the area of the between-shell interface, and Δr is the inter-shell distance.

Similar equations described diffusion of the WT HPCA, HPCA-Ca, and HPCA-2Ca as well as the corresponding forms of the mutant (HPCAmut, HPCAmut-Ca, and HPCAmut-2Ca).

The initial concentrations of the WT and mutant HPCA, Ca^{2+}, their forward (k_{fi}) and backward (k_{bi}) kinetic rates of reactions i = 1,2,3 are given in Table 1.

Simulation of sAHP potassium current. Solving the above translocation equations gave concentrations of membrane fractions of HPCA and mutant, $HPCA_{\text{membr}}$ and $HPCAmut_{\text{membr}}$. These values were further used to determine the sAHP potassium current activated by HPCA and mutant translocated to the plasma membrane. The current was described as:

$$J_K = G_K\cdot n\cdot(V - E_K)$$

where G_K = 60 mS/cm^2 and E_K = −90 mV are, respectively, maximum conductivity and reversal potential of the current; n is kinetic variable of HPCA- and HPCAmut-dependent activation. The following equations described n:

$$dn/dt = (n_\infty - n)/\tau_n;\ \tau_n = 1/(Q_{10}\cdot(\alpha_n + \beta_n))$$

$$n_\infty = \alpha_n\cdot\tau_n;\ \alpha_n = Ra\cdot(HPCA_{\text{membr}} + HPCAmut_{\text{membr}})$$

$$Ra = 0.01\ \text{mM}^{-1}\cdot\text{ms}^{-1};\ \beta_n = Rb = 0.02\ \text{mM/ms}$$

Kinetic constants of HPCA and N75K mutant interaction with Ca^{2+} and plasma membrane (k_{fi} and k_{bi}, i = 1, 2, 3 in Table 1) were fitted in order to reproduce amplitudes and decays of translocation transients observed in our experiments (see below Fig. 3B, 4B, 7Ab, Ac). The constants in the above equations relating the AHP conductance and amount of HPCA translocated to the plasma membrane (Ra and Rb) were also fitted according to measurements of sAHP current (see below Fig. 6, 7Ac).

The conductance of somatically located receptors, which were tonically activated by gliotransmitters (Rose et al., 2017) was set to 0.25 mS/cm^2 (Fig. 7Ba, Bb) or varied (Fig. 7Bc).

A transient activation of glutamatergic conductance, Gs, evoking a burst of somatic APs (Fig. 7C, D) was simulated by an induction of Gs transient having an asymmetrical bell-shaped time course described by a NEURON standard "alpha-function":

$$Gs(t) = Gsmax\ [(t - t_0)/\tau]\exp[-(t - t_0 - \tau)/\tau]$$

where t, t_0, and τ are respectively time, onset moment, and characteristic time constant; $Gsmax$ is maximum Gs (Hines and Carnevale, 2001).

In all above equations $Q_{10} = 2.3^{(t^\circ - 36)/10}$ is the temperature factor, where t° is the temperature in Celsius degrees (36 °C in our simulation experiments).

3. Results

3.1. Dystonic mutations modify Ca^{2+}-binding properties of HPCA

HPCA is a powerful Ca^{2+} buffer that contributes up to 100 μM to a cytosolic Ca^{2+} buffer capacity (Raghuram et al., 2012). Heterologous expression of HPCA or its dystonic mutants in HEK cells was employed in order to clarify whether N75K and T71N dystonic mutations in the EF-hand 2 could impair Ca^{2+} binding of the mutants thereby decreasing a cytosolic Ca^{2+} buffer capacity of the cells. The HEK cells were chosen for this set of experiments since they closely resemble adrenal chromaffin cells, whose Ca^{2+} buffer capacity (Neher and Augustine, 1992) is substantially lower than that of neurons (Belan et al., 1993; Fierro and Llano, 1996; Lee et al., 2000) mainly used in this work. We suggested that an additional exogenous Ca^{2+} buffer introduced by the heterologous HPCA expression could produce stronger influence on the decay kinetics of $[Ca^{2+}]_i$ transients in cells having lower Ca^{2+} buffer capacity (Foehring et al., 2009; Helmchen et al., 1996).

First, we estimated if HPCA expression increased a cytosolic Ca^{2+} buffer capacity substantially enough to be resolved as significant changes in the decay kinetics of $[Ca^{2+}]_i$ transients. For this, the HEK cells were transfected with WT HPCA tagged by CFP; afterwards both transfected and non-transfected (NT) cells in the same cultures were loaded with 'caged' Ca^{2+}, NP-EGTA AM, and Ca^{2+}-dye, Fura Red AM. $[Ca^{2+}]_i$ transients were induced by several consequent UV-flashes and measured in both WT HPCA transfected and NT neurons in the same field of view (Fig. 1A). Decays of $[Ca^{2+}]_i$ transients in cells expressing WT HPCA were significantly slower than ones in NT cells as shown by a higher level of residual $[Ca^{2+}]_i$ (Fig. 1B, C; 0.34 ± 0.02 and 0.17 ± 0.01 for $\Delta F/F$ at 80 s for WT HPCA transfected and NT HEK cells, respectively, $p < .001$, $n_{WT} = 10$ and $n_{NT} = 16$, four different cultures). Thus, introduction of exogenous HPCA firmly established an increase in Ca^{2+} buffer capacity of HEK cells as measured by the decay kinetics of the $[Ca^{2+}]_i$ transients. The magnitude of change was substantial indicating that effects, if any, of the dystonic mutants could also be resolved in this system.

As the next step, we investigated if expression of DYT2 mutants in HEK cells resulted in a decreased Ca^{2+} buffer capacity compared to the expression of WT HPCA. The same HEK cultures were sequentially transfected with WT HPCA-CFP and dystonic mutants tagged by YFP. This procedure allowed us to have cells transfected with either WT HPCA or its dystonic mutant (< 5% of transfected cells for each group) in the same cultures and the same fields of views. We found that a decay of $[Ca^{2+}]_i$ transients was significantly faster in cells expressing N75K mutant compared to the cells expressing WT HPCA (Fig. 1D–F, 0.35 ± 0.02 vs 0.20 ± 0.02 at 80 s for WT HPCA and N75K mutant, respectively; $p < .01$, $n_{WT} = 11$ and $n_{N75K} = 11$; four cultures). At the same time, we did not observe a significant difference in this parameter between WT HPCA and T71N mutant (Fig. 1G–I, 0.33 ± 0.02 and 0.29 ± 0.03 for $\Delta F/F$ at 80 s for WT HPCA and T71N, respectively; $p = .46$, $n_{WT} = 12$ and $n_{T71N} = 23$, 5 cultures). These results demonstrate a decreased total Ca^{2+} buffer capacity of N75K mutant compared to the WT HPCA for a studied range of $[Ca^{2+}]_i$.

The Ca^{2+} buffer capacity is a function of $[Ca^{2+}]_i$ (Neher and Augustine, 1992). If Ca^{2+} binding in dystonic mutants at EF-hand 2 was preserved but with a lower affinity, then Ca^{2+} buffering by mutants at higher levels of $[Ca^{2+}]_i$ could be relatively stronger than at the basal one. We validated this hypothesis using an experimental design with Ca^{2+} uncaging by four flashes of UV light with an interflash interval of 8 s. Since Ca^{2+} extrusion is very slow in HEK cells, these flashes resulted in four increased and almost constant levels of $[Ca^{2+}]_i$ (Fig. 1J). As above, these experiments were conducted paired wise for the same cultures and the same fields of view for WT HPCA-CFP versus its dystonic mutants tagged by YFP. Levels of $[Ca^{2+}]_i$ were normalized to its level after the final flash for each cell. We found a significantly higher

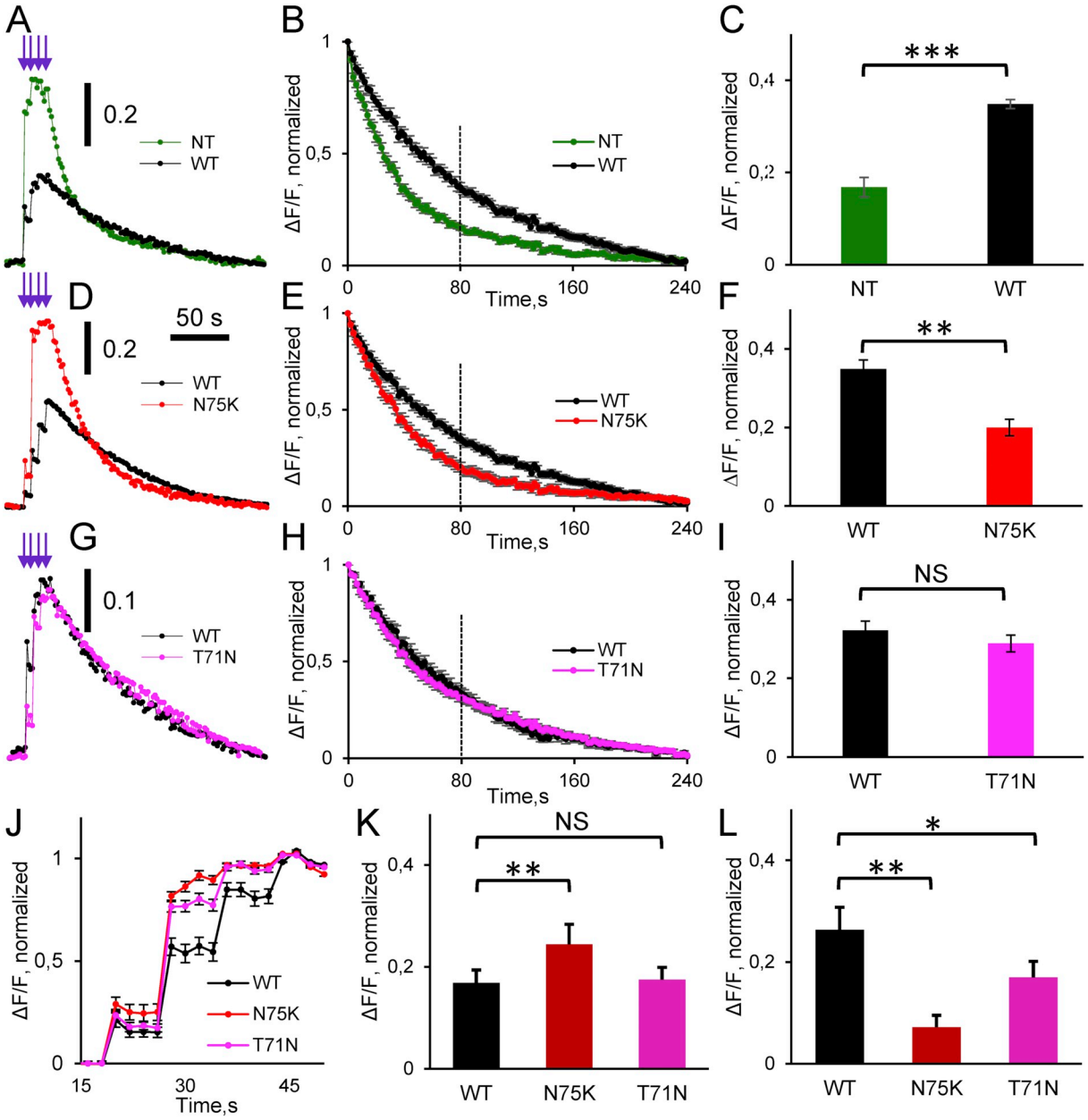

Fig. 1. Decreased Ca^{2+} buffer capacity of N75K mutant compared to wild type HPCA.
A. Time course of $[Ca^{2+}]_i$ transients induced by Ca^{2+} uncaging for representative non-transfected (NT, green) and wild type HPCA transfected (WT, black) cells. Here and in other panels, purple arrows indicate moments of consecutive Ca^{2+} uncaging. Vertical bars in A, D, and G indicate relative changes in Fura Red fluorescence induced by the uncaging; the changes were calculated as *ΔF/F*. B. Pooled results of experiments represented in A demonstrate that a decay of $[Ca^{2+}]_i$ transients induced by the uncaging is slower in WT transfected compared to NT cells. Dotted lines in B, E, and H denote moments, for which data were compared in C, F, and I, respectively. Y axis in this and other panels represents *ΔF/F* normalized for each trace to its maximal value. C. $[Ca^{2+}]_i$ decay after uncaging is faster in NT cells demonstrating a higher cytosolic Ca^{2+} buffer capacity in WT cells. D-F. Time course of $[Ca^{2+}]_i$ transients induced by Ca^{2+} uncaging (D) and their decay (E), which is slower in WT (black) than N75K (red) transfected cells (F) demonstrating a lower Ca^{2+} buffer capacity in N75K cells. G-I. No significant difference in decays of $[Ca^{2+}]_i$ transients is observed in cells expressing WT HPCA and its T71N mutant. J. Normalized $[Ca^{2+}]_i$ elevations induced by repeated uncagings in cells expressing WT HPCA and its dystonic mutants. K. Amplitudes of normalized $[Ca^{2+}]_i$ elevations in response to the first uncaging. The amplitudes in cells expressing N75K are significantly higher showing that relative N75K mutant ability to bind Ca^{2+} near a basal level of $[Ca^{2+}]_i$ is lower compared to one of the other proteins. L. The amplitudes of normalized $[Ca^{2+}]_i$ elevations in response to the third uncaging demonstrating a significantly lower relative increase in cells expressing N75K. This result implies relatively higher ability of N75K to bind Ca^{2+} when $[Ca^{2+}]_i$ is increased. (For interpretation of the references to colour in this figure legend, the reader is referred to the web version of this article.)

relative increase of $[Ca^{2+}]_i$ in response to the first flash in cells expressing N75K mutant compared to both cells expressing the WT HPCA and its T71N mutant (Fig. 1J, K; 0.17 ± 0.03, $n = 27$ for WT HPCA, 0.18 ± 0.02, $n = 26$ for T71N and 0.28 ± 0.04, $n = 11$ for N75K; $p < .05$ for N75K vs T71N; $p < .01$ for N75K vs WT HPCA), indicating to the lower relative Ca^{2+} buffer capacity of N75K at a basal level of $[Ca^{2+}]_i$. Interestingly, we observed an opposite result after third uncaging; namely, a difference between normalized levels of $[Ca^{2+}]_i$ after the third uncaging was significantly larger in cells expressing WT HPCA compared to ones expressing both T71N (Fig. 1J, L, 0.26 ± 0.02, n = 27 for WT HPCA vs 0.17 ± 0.02, n = 26 for T71N, $p < .05$) and N75K mutants (Fig. 1J, L 0.26 ± 0.02, n = 27 for HPCA vs

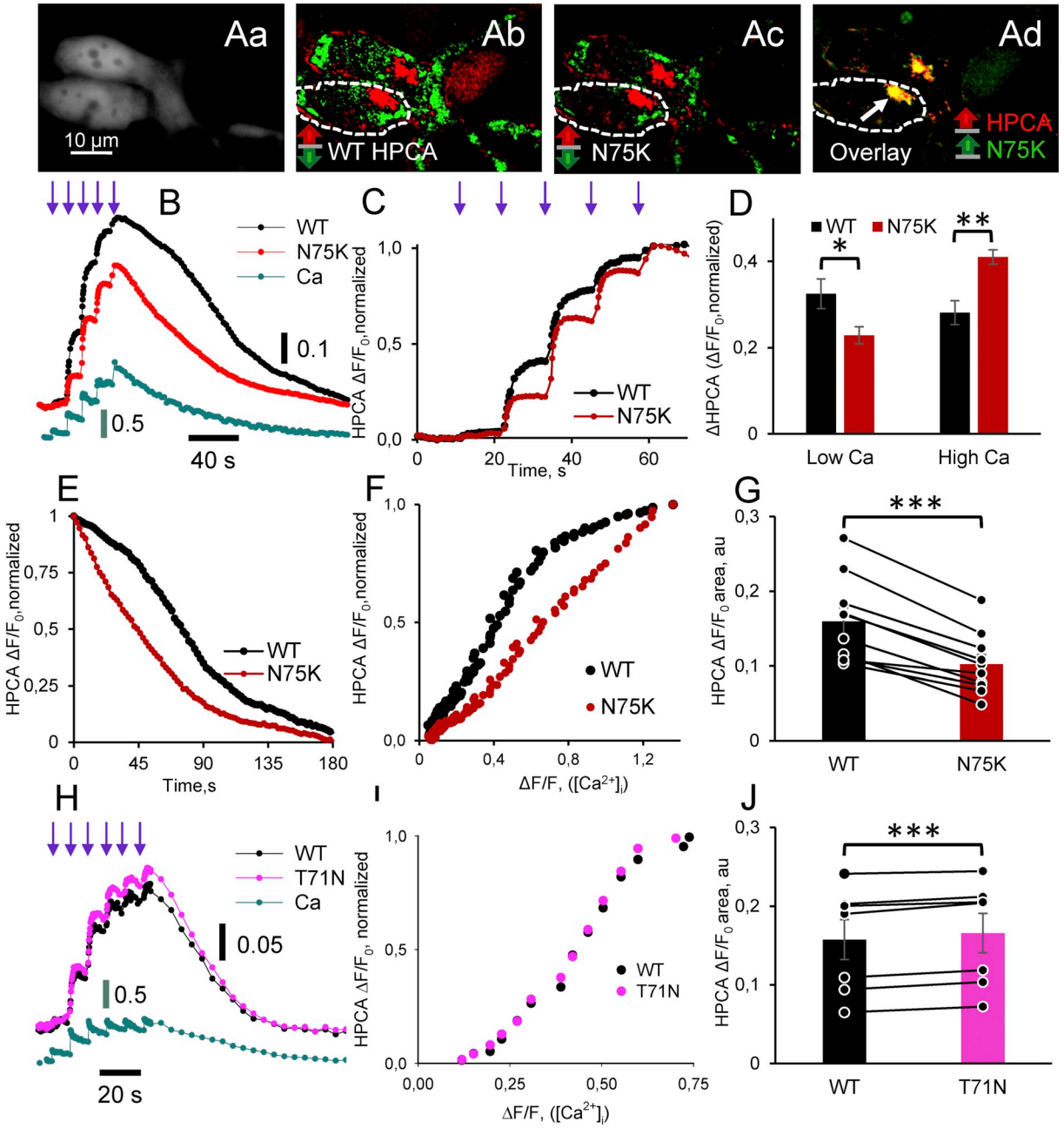

Fig. 2. N75K mutant revealed reduced Ca^{2+}-sensitivity compared to wild type HPCA.

Aa. A fluorescent image of HEK cells co-expressing WT HPCA–CFP and N75K–YFP recorded in CFP emission channel. Ca^{2+} uncaging induced $[Ca^{2+}]_i$ transients (green trace in B) leading to translocation of WT HPCA–CFP (Ab) and N75K–YFP (Ac) to certain sites within the cells. Red and green pixels represent sites, in which $[Ca^{2+}]_i$ transients induced an increase and decrease in a protein concentration, respectively, reflecting the protein translocation. Ad. An overlay of WT HPCA–CFP and N75K–YFP translocation shown in Ab and Ac. Red and green colors represent an increase WT HPCA–CFP or N75K–YFP concentrations, respectively. Note co-localization of translocation sites for both proteins revealed in yellow. B. Time courses of $[Ca^{2+}]_i$ transients (green trace) and Ca^{2+}-dependent translocation of WT HPCA-CFP (black trace) and N75K-YFP (red trace) induced by consecutive Ca^{2+} uncagings. Results in B, C, E and F are shown for a region of interest indicated by a white arrow in Ad. A black vertical scale bar represents relative changes ($\Delta F/F_0$) in protein fluorescence in this region. Onsets of uncagings induced by UV flashes are indicated by purple arrows. Note a substantially higher amplitude of WT HPCA-CFP translocation as well as stronger translocation to the second and third uncagings compared to one of N75K-YFP. C. Normalized time course of translocation rising phase shown in B. Y axis in C, F and I represents changes in $\Delta F/F_0$ normalized for each trace to its maximal value. D. Pooled results demonstrating opposite changes in relative translocation amplitudes for WT HPCA-CFP and N75K-YFP in response to the first two (Low Ca) and last two (High Ca) uncagings. This result indicates to higher relative Ca^{2+} sensitivity of WT-HPCA compared to N75K near a basal level of $[Ca^{2+}]_i$. ΔHPCA in Y axis represents an increase in normalized HPCA $\Delta F/F_0$ shown in C in response to the second and fourth uncaging. E. Normalized time courses of translocation decays shown in B demonstrating the faster decay of N75K translocation. F. $[Ca^{2+}]_i$–dependence of normalized translocation for WT HPCA and N75K demonstrating a decreased ability of N75K for translocation at $[Ca^{2+}]_i$ close to its basal level. $\Delta F/F$ ($[Ca^{2+}]_i$) is proportional to $[Ca^{2+}]_i$ and represents changes in Fura Red fluorescence induced by Ca^{2+} uncaging, ΔF, divided by a value of fluorescence, F (see 2.7 in Methods). G. Pooled results for $[Ca^{2+}]_i$–dependency of translocation demonstrating lower Ca^{2+} sensitivity of N75K compared to WT HPCA. Each pair of connected points represents areas under dependence of $\Delta F/F_0$ for WT HPCA and N75K translocation on $\Delta F/F$ ($[Ca^{2+}]_i$) for a particular co-transfected neuron. H, I, J. Almost similar $[Ca^{2+}]_i$–dependency of translocation was observed for WT HPCA and T71N. (For interpretation of the references to colour in this figure legend, the reader is referred to the web version of this article.)

0.07 ± 0.02, n = 11 for N75K, $p < .01$). These results show that Ca^{2+} buffering of WT HPCA decreases while one of N75K increases when $[Ca^{2+}]_i$ increases.

Thus, the WT HPCA has a larger total Ca^{2+} buffer capacity than N75K mutant in a studied range of $[Ca^{2+}]_i$ and its buffer capacity is relatively larger at the basal rather than higher levels of $[Ca^{2+}]_i$ contrary to N75K mutants. The latter also indicates that WT HPCA affinity for Ca^{2+} is higher than one of its dystonic N75K mutant.

3.2. N75K mutation modifies HPCA biophysical properties

Our results demonstrate that the dystonic mutants have different biophysical properties compared to WT HPCA (Fig. 1). Thus, these mutations may lead to changes in Ca^{2+}-dependency, value and kinetics of HPCA translocation from the cytosol to the membranes. They may even affect a Ca^{2+}-myristoyl switch (Ames et al., 1997) resulting in complete lack of translocation of HPCA. Therefore, we studied how dystonic mutations affect HPCA translocation to the membranes in HEK cells. For that, HEK cells were co-transfected with WT HPCA tagged by CFP and one of the dystonic mutants tagged by YFP. Increases in $[Ca^{2+}]_i$ were induced by Ca^{2+} uncaging from NP-EGTA by a series of UV-flashes (5–6 flashes of 0.5 s with interflash interval of 2–10 s) and measured by Fura Red. Thus, the expressed pair of proteins were subjected in each given cell to the same spatio-temporal patterns of $[Ca^{2+}]_i$ changes allowing to directly compare Ca^{2+}-dependency, value and kinetics of protein translocation.

Both WT HPCA and mutants were homogenously (data not shown) and cytosolically (Dovgan et al., 2010; O'Callaghan et al., 2003) distributed over the cells with exception of some small organelles (Fig. 2Aa). Step-like increases in $[Ca^{2+}]_i$ induced by the uncaging led to WT HPCA and mutant translocation to both the plasma membrane and some intracellular organelles (Fig. 2Ab, Ac, B, H), indicating that Ca^{2+}-myristoyl switch remained, at least partially, preserved in both mutants. The translocation occurred to the same membrane loci (Fig. 2Ab, Ac, Ad) indicating to higher affinity of both HPCA and its mutants to the same cellular membranes. However, we found that the value of translocation for N75K (Fig. 2B) rather than for T71N (Fig. 2H) mutant was significantly lower than for WT HPCA (Fig. 2B, 0.14 ± 0.03 vs 0.06 ± 0.01 for the first two increase in $[Ca^{2+}]_i$ and 0.44 ± 0.07 vs 0.29 ± 0.06 for a whole set of increases in $[Ca^{2+}]_i$ ($n = 9$, $p < .001$) for WT HPCA and N75K mutant, respectively). These results directly demonstrate abnormal N75K signaling by means of translocation to the membranes that was most strongly manifested near the basal level of $[Ca^{2+}]_i$. When translocation transients were normalized to their amplitude values (Fig. 2C), it appeared that the first two uncaging events led to substantially larger relative translocation for WT HPCA compared to N75K (Fig. 2D, 32 ± 3% vs 22 ± 2%, $n = 5$, $p < .05$, for WT HPCA and N75K, respectively), while the fourth and fifth uncaging events led to the relatively larger translocation of N75K mutant compared to the WT HPCA (Fig. 2D, 28 ± 3% vs 41 ± 2%, n = 5, $p < .01$ for WT HPCA and N75K, respectively). It suggests that the WT HPCA is relatively more sensitive to Ca^{2+} at a basal level of $[Ca^{2+}]_i$ than N75K and supports our previous conclusion (Fig. 1L) that the WT HPCA affinity for Ca^{2+} is higher than one for N75K.

Next, we investigated a steady-state $[Ca^{2+}]_i$-dependence of translocation for HPCA and its mutants in the whole range of $[Ca^{2+}]_i$ available when uncaging was engaged. We took advantage of slow decays of $[Ca^{2+}]_i$ transients in HEK cells, lasting up to 2–3 min (Figs. 1, 2B, H). Since processes related to HPCA translocation are almost two orders of value faster (Dovgan et al., 2010; Markova et al., 2008), it allows the proteins under study to reach quasi-equilibrium state in regards to Ca^{2+} concentration during the decays. Taking this into account, we directly showed that the translocation was larger for WT HPCA compared to N75K mutant in the whole range of $[Ca^{2+}]_i$ under study (Fig. 2B, 0.44 ± 0.06 vs. 0.29 ± 0.06, for amplitudes of WT HPCA and N75K translocation transients, respectively, $p < .001$, n = 9). Normalization of translocation transients also demonstrated a faster decay for N75K translocation (Fig. 2E; 38.3 ± 1.6 s vs. 26.3 ± 2.4 s, for weighted τ of WT HPCA and N75K translocation transients, respectively, $p < .001$, n = 9). At the same time, no substantial differences in amplitudes (0.20 ± 0.02 vs. 0.24 ± 0.03 for WT HPCA and T71N, $p < .01$, $n = 7$) and decay kinetics (19.5 ± 3.2 vs. 20.6 ± 3.4, for WT HPCA and T71N, $p < .05$, n = 7) were observed for T71N mutant (Fig. 2H).

Simultaneous measurements of protein translocation and $[Ca^{2+}]_i$ (Fig. 2B, H) allowed us to build the normalized $[Ca^{2+}]_i$-dependencies of protein translocation (Fig. 2F, I). These dependencies directly demonstrate decreased ability of N75K (Fig. 2F) rather than T71N (Fig. 2I) to translocate at $[Ca^{2+}]_i$ close to its basal level.

Additionally, we measured areas under dependence of WT HPCA and N75K translocation on $[Ca^{2+}]_i$ for co-transfected neurons (data not shown) that represent cumulative ability of respective proteins to translocate in the studied range of $[Ca^{2+}]_i$. The area was substantially smaller for N75K compared to WT HPCA (Fig. 2G; 0.16 ± 0.02 vs 0.10 ± 0.01 for WT and N75K, respectively, $p < .001$, $n = 10$) while it was similar for WT HPCA and T71N mutant (Fig. 2J, 0.16 ± 0.03 vs 0.17 ± 0.02 for WT and T71N, respectively, $p < .001$, n = 7).

Altogether, our data indicate that both Ca^{2+}-myristoyl switch and translocation selectivity to certain membranes were not substantially affected by DYT2 mutations. At the same time, N75K mutant has impaired Ca^{2+}-sensitivity resulting in a significant decrease in the protein translocation to the membranes.

3.3. N75K mutation perturbs Ca^{2+}-dependent HPCA translocation in hippocampal neurons

Spatio-temporal patterns of $[Ca^{2+}]_i$ changes induced by Ca^{2+} uncaging in HEK cells are different from ones evoked in neurons by activation of voltage- and ligand-gated Ca^{2+} channels. Besides, a phospholipid content of inner leaflet of the neuronal plasma membrane determining its affinity to HPCA is likely to be different from one of the Golgi network and plasma membrane of HEK cell. Therefore, at the next step we checked how changes in biophysical properties induced by N75K mutation affect Ca^{2+}-dependent WT HPCA translocation in hippocampal neurons. Since sAHP conductance is most likely localized to the proximal part of apical dendrite (Power et al., 2011), HPCA translocation were studied in this part of dendritic tree. For that purpose, we co-transfected neurons in primary hippocampal cultures with WT HPCA-CFP and N75K-YFP constructs. The transfected neurons were patched in the whole cell configuration and $[Ca^{2+}]_i$ transients were induced by membrane depolarization from −70 to 0 mV. The induced $[Ca^{2+}]_i$ transients resulted in significantly stronger translocation of WT HPCA compared to N75K in response to a wide range of depolarization durations (Fig. 3A–D). The difference in the amplitudes of translocation transients was especially prominent during short depolarizations (e.g. 3-fold at 0.25 s, Fig. 3B, E (top), $p < .01$, $n = 6$) producing fast and low $[Ca^{2+}]_i$ transients (data not shown). However, we did not observe a significant difference in the amplitudes of translocation between WT HPCA and N75K during a prolonged depolarization (4.0 s, Fig. 3E (bottom); $p = .88$) resulting in $[Ca^{2+}]_i$ transients of high amplitude and long duration (data not shown). Additionally, the mutant and WT protein translocated to the same sites of the plasma membrane (yellow regions in Fig. 3Ad). These latter results confirm that N75K mutation did not substantially affect Ca^{2+}-myristoyl switch, protein affinity to the plasma membrane and, hence, HPCA targeting. At the same time, the WT HPCA stronger translocated at lower $[Ca^{2+}]_i$ compared to N75K mutant confirming a decreased $[Ca^{2+}]_i$ sensitivity induced by N75K mutation.

Important properties of HPCA and its mutants are kinetics of rise and decay of translocation transients. They characterize biophysical properties of protein interaction with both Ca^{2+} and plasma membrane and most probably determine the kinetics of sAHP, which is controlled

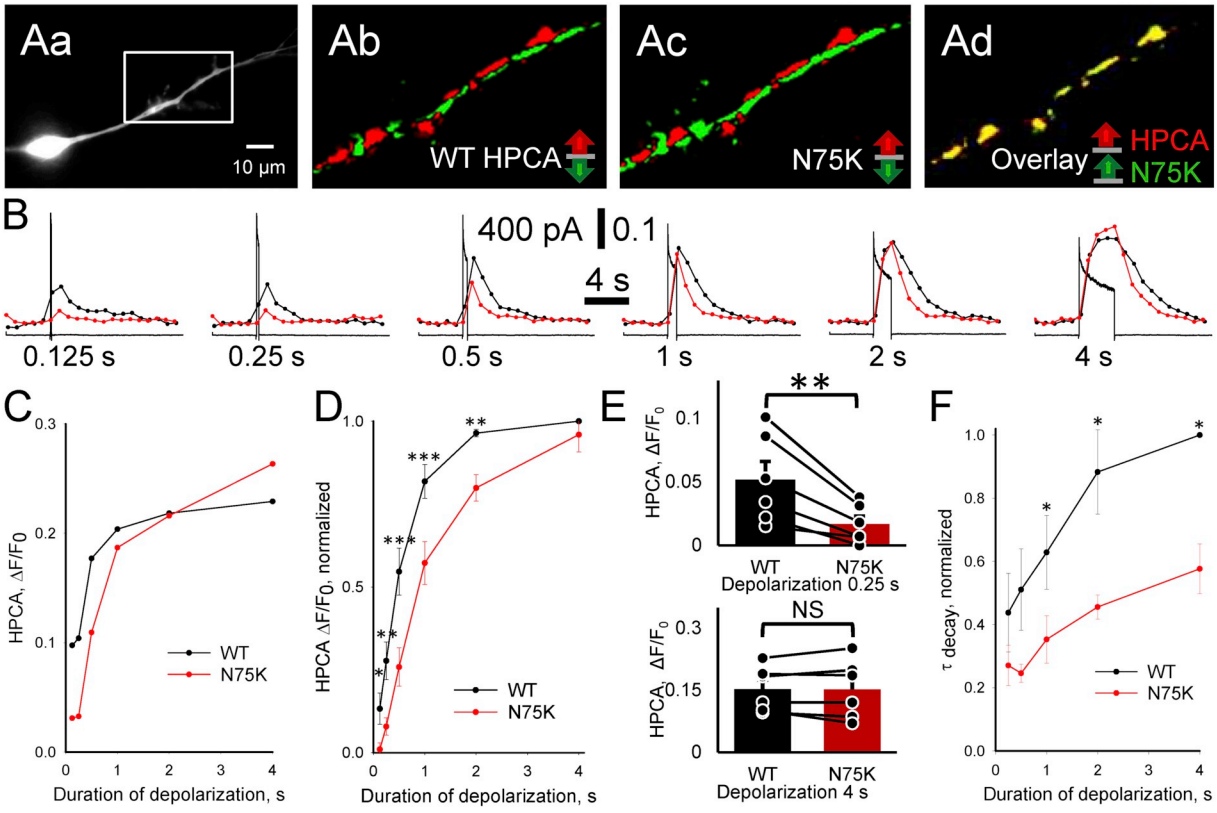

Fig. 3. Ca^{2+}-dependent translocation of N75K mutant in hippocampal neurons is decreased compared to WT HPCA.
Aa. A fluorescent image of a representative hippocampal neuron co-expressing WT HPCA–CFP and N75K–YFP recorded in CFP emission channel. The region in the white box is enlarged in Ab-Ad. Translocation sites for WT HPCA–CFP (Ab) and N75K–YFP (Ac) in the dendritic tree in response to neuronal depolarization from −70 to 0 mV (1 s) are shown in red. Ad. An overlay of WT HPCA–CFP and N75K–YFP translocation sites is shown in yellow indicating a similar spatial pattern of proteins' translocation. B. Time courses of WT HPCA-CFP (dotted black) and N75K-YFP (red) translocation and transmembrane currents (black) evoked by step depolarization (from −70 to 0 mV) of different durations in a neuron depicted in A. A black vertical scale bar represents relative changes ($\Delta F/F_0$) in protein fluorescence in the regions shown in red in Ab and Ac. Note substantially weaker N75K–YFP translocation for short durations of depolarization. C. Translocation amplitudes plotted against durations of depolarization for WT HPCA-CFP and N75K–YFP for the same neuron. D. Pooled results for dependence of normalized translocation amplitude on depolarization duration demonstrating perturbed ability of N75K mutant to translocate. E. Upper histogram: Decrease of translocation amplitudes for N75K–YFP compared to WT HPCA-CFP in case of short depolarization (small and fast increase of $[Ca^{2+}]_i$). Lower histogram: similar translocation amplitudes for both proteins in case of prolonged depolarization (large and prolonged increase of $[Ca^{2+}]_i$) demonstrating a complete preservation of Ca^{2+}-myristoyl switch in N75K mutant. F. Pooled results for normalized decay time of translocation transients showing significantly faster decay of N75K-YFP translocation compared to WT HPCA-CFP. (For interpretation of the references to colour in this figure legend, the reader is referred to the web version of this article.)

by HPCA translocated to the plasma membrane (Andrade et al., 2012; Kim et al., 2012; Tzingounis et al., 2007). The rise time is mainly determined by kinetics of Ca^{2+} binding and protein diffusion to the plasma membrane. These processes occur in a subsecond range (Faas and Mody, 2012) and a low acquisition rate (1 Hz) engaged in our experiments to decrease photobleaching did not allow us to observe a possible difference in a translocation rise time between these two proteins (data not shown). At the same time, we found that the decay of N75K translocation transients is significantly faster compared to one of HPCA in the whole range of durations of depolarization (Fig. 3F). For example, translocation decay times were 10.9 ± 1.9 s and 5.9 ± 1.2 s for HPCA and N75K, respectively ($p < .001$, n = 6), after depolarization of 2.0 s. The decay time increased with increasing the duration of depolarization reflecting its $[Ca^{2+}]_i$ dependence for both proteins (Fig. 3F). At the same time, we found that even though the translocation decay times for both proteins increased during longer depolarizations, their ratio was not changed substantially (Fig. 3F), indicating to a faster unbinding rate from the plasma membrane for N75K mutant compared to the WT protein.

3.4. Short bursts of action potentials do not produce N75K translocation

Having established changes in biophysical properties of HPCA induced by N75K mutation in a range of $[Ca^{2+}]_i$, which can be potentially observed in the hippocampal neurons, we further investigated how these changes affect HPCA translocation evoked by physiologically relevant neuronal activity. HPCA translocation filters out short-lasting $[Ca^{2+}]_i$ transients even if they have large amplitudes and integrates prolonged elevation of $[Ca^{2+}]_i$ (Dovgan et al., 2010; Markova et al., 2008). For example, a single action potential leading to a large and short elevation of $[Ca^{2+}]_i$, (decay of 12 ms (Sabatini et al., 2002)) in a neuronal dendritic tree does not produce a visible HPCA translocation in the dendrites of hippocampal neurons (Markova et al., 2008). Thus, we decided to study a difference in translocation between HPCA and its N75K mutant by inducing trains of action potentials (5 to 100 action potentials at 50 Hz). Trains in a range of 5–20 action potentials resemble intrinsic neuronal discharges while longer trains may occur in some pathological conditions (Madison and Nicoll, 1984; Parrilla-Carrero et al., 2018). We hypothesized that lower Ca^{2+}-sensitivity and faster unbinding rate of the N75K mutant should result in severe abnormalities of its Ca^{2+}-dependent signaling. Since discharges of action potentials produce sAHP via HPCA translocation to the plasma membrane (Andrade et al., 2012; Kim et al., 2012; Tzingounis et al., 2007), we wondered if the mutant did translocate during short trains of action potentials. For that, trains of action potentials were induced in hippocampal neurons co-transfected with WT HPCA-CFP and N75K-YFP by

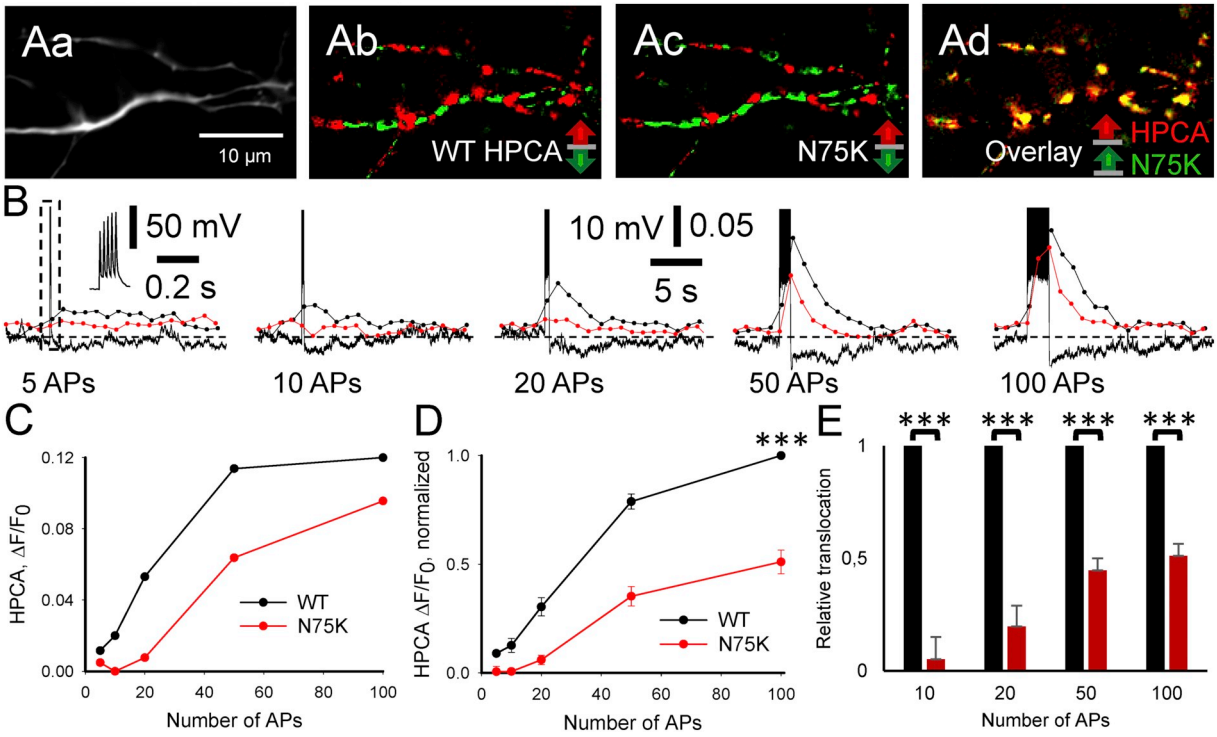

Fig. 4. Short trains of action potentials do not produce N75K translocation.
Aa. A fluorescent image of the proximal dendritic tree of a representative hippocampal neuron co-expressing WT HPCA–CFP and N75K–YFP (CFP emission channel). Translocation of WT HPCA–CFP (Ab) and N75K–YFP (Ac) to the plasma membrane in the neuronal dendritic tree in response to a burst of 50 APs (50 Hz) are shown in red. Ad. An overlay of WT HPCA–CFP and N75K–YFP translocation sites is shown in yellow indicating a similar spatial pattern of proteins' translocation. B. Time courses of WT HPCA-CFP (dotted black) and N75K-YFP (red) translocation and membrane potential (black) evoked by AP bursts in a neuron depicted in A demonstrating substantially weaker N75K–YFP translocation. A black vertical scale bar represents relative changes ($\Delta F/F_0$) in protein fluorescence in the regions shown in red in Ab and Ac. Note slow afterhyperpolarization, sAHP, induced by the bursts. Dashed lines demonstrate a holding level of membrane potential. C. Translocation amplitudes plotted against the number of APs in the bursts for WT HPCA-CFP and N75K–YFP for the same neuron. D. Pooled results for dependence of normalized translocation amplitude on the number of APs in the bursts. E. Perturbed translocation of N75K mutant. N75K-YFP translocation amplitudes normalized to ones of WT HPCA-CFP. Note absence of N75K-YFP translocation in response to bursts having < 10 APs. (For interpretation of the references to colour in this figure legend, the reader is referred to the web version of this article.)

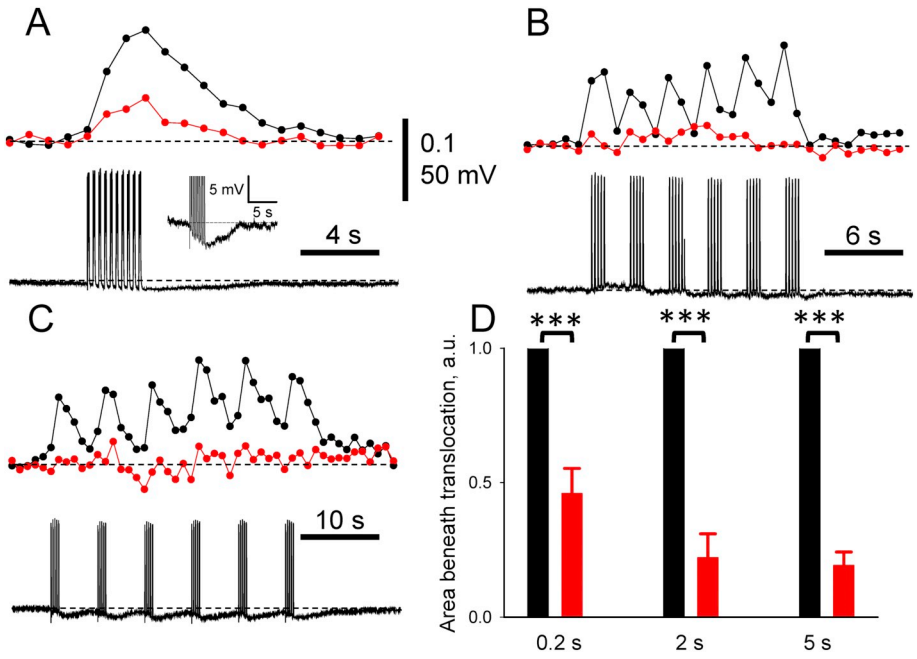

Fig. 5. Impaired translocation of N75K mutant in response to theta-burst stimulation.
A. WT HPCA-CFP (dotted black) and N75K-YFP (dotted red) translocation evoked in a co-transfected neuron by two theta-bursts separated by a 0.2 s interval demonstrating substantially weaker N75K–YFP translocation. A black vertical scale bar represents relative changes ($\Delta F/F_0$) in protein fluorescence in translocation sites. An insert demonstrates sAHP observed after the theta-bursts. B, C. Impaired integration of theta-bursts by N75K translocation at 2 and 5 s interburst interval. Bottom black traces represent changes in the neuronal membrane potential. The dashed lines in A-C demonstrate basal levels of proteins' fluorescence and holding potential. Note sAHP (A-C) induced in the neurons by the theta-bursts and coinciding with HPCA translocation. D. Pooled results for areas under N75K-YFP translocation transients, normalized to respective areas for WT HPCA-CFP translocation, demonstrating abnormal integration of rhythmic neuronal activity by N75K mutant. (For interpretation of the references to colour in this figure legend, the reader is referred to the web version of this article.)

depolarizing current stimuli (Fig. 4A, B). We did observe robust translocation of the WT HPCA in response to short trains of action potentials (5–20 APs), while the mutant translocation was almost absent (Fig. 4A–D). For example, HPCA translocation reached 30 ± 4% of maximal value after 20 action potentials (Fig. 4D; $n = 11$) and its amplitude was about 6-fold higher than that of N75K translocation (Fig. 4E; n = 11).

Longer trains induced translocation of both WT HPCA and N75K (Fig. 4A–D) although the amplitudes of N75K translocation were still lower (Fig. 4C, D; 0.51 ± 0.05% for WT HPCA and N75K, respectively, after 100 action potentials, $p < .001$, n = 11). As in the case of the previously obtained data (Figs. 2, 3), both the WT HPCA and mutant translocated to the same sites in the dendritic plasma membrane (Fig. 4Ab, Ac, Ad).

These results indicate that during the most relevant type of neuronal activity, short action potential bursts, N75K mutant does not translocate to the plasma membrane, effectively and completely filters out this type of activity. Since HPCA can act as a neuronal Ca^{2+} sensor to modulate its membranous targets (including sAHP conductance) only after translocation to the plasma membrane, N75K mutation most probably results in a loss of function of the mutant during this type of neuronal activity.

3.5. N75K mutant abnormally translocates during theta burst stimulations

It has been shown that HPCA is capable of integrating $[Ca^{2+}]_i$ increases induced by repetitive discharges or tonic activity into its increasing translocation to the plasma membrane (Dovgan et al., 2010; Markova et al., 2008). If a value of sAHP conductance is proportional to an amount of translocated HPCA, then the integration would contribute to sAHP induced by repetitive discharges. Since we established that N75K mutant had faster unbinding rate from the plasma membrane and lower sensitivity to Ca^{2+} compared to HPCA, we hypothesized that N75K mutation impaired integration of repetitive $[Ca^{2+}]$i elevations. To check this hypothesis, neurons were subjected to theta burst stimuli (TBS) (Larson and Munkácsy, 2015; Widman et al., 2018), each containing 5 trains of 5 APs at 100 Hz separated by 0.2 s. A time interval between theta bursts was set to 0.2, 2, 5 and 20 s (Fig. 5). Areas under translocation transients were chosen to quantitatively compare cumulative values of translocation for both proteins.

We found that both WT HPCA and N75K mutant can integrate $[Ca^{2+}]_i$ transients by translocation to the plasma membrane throughout two TBS separated by 0.2 s (Fig. 5A). The area under N75K translocation transients were significantly smaller compared to ones under HPCA translocation transients (~2-fold, Fig. 5A, D, $p < .001$, $n = 6$) demonstrating that although N75K is capable of integration of theta-burst activity at a short intertrain interval, this integration is impaired. At the intermediate intervals of 2 and 5 s, not only the area under N75K translocation transients was lower (~5-fold, Fig. 5B–D, $p < .001$, $n = 5$ for B and 2 for C), but the integration of the TBS was almost absent for N75K mutant. While N75K responded to each theta-burst with no or small transient translocation, HPCA was bound to the plasma membrane between the bursts and gradually accumulated during the TBS, effectively integrating the neuronal activity (Fig. 5B, C). It is important to note that the theta bursts also led to induction and summation of sAHP in a proportion of tested neurons (Fig. 5A–C). At 20 s interval between theta-bursts, both WT HPCA and N75K responded to each theta-burst by clearly separated transient translocation (as shown in Fig. 4B) and were unable to integrate the theta-bursts (data not shown).

Altogether these results indicate that N75K mutation lead to abnormal integration of rhythmic neuronal activity by HPCA translocation to the plasma membrane that is likely to upregulate this activity since the translocation gates sAHP (Tzingounis et al., 2007).

3.6. N75K mutant does not control sAHP current

Next, we investigated if N75K mutation affected gating of sAHP. Our results showed that sAHP was observed in neurons expressing N75K (Figs. 4B, 5A–C) indicating that N75K did not prevent endogenous and exogenous HPCA to gate sAHP. The mutant also translocated to the same sites in the plasma membrane as WT HPCA

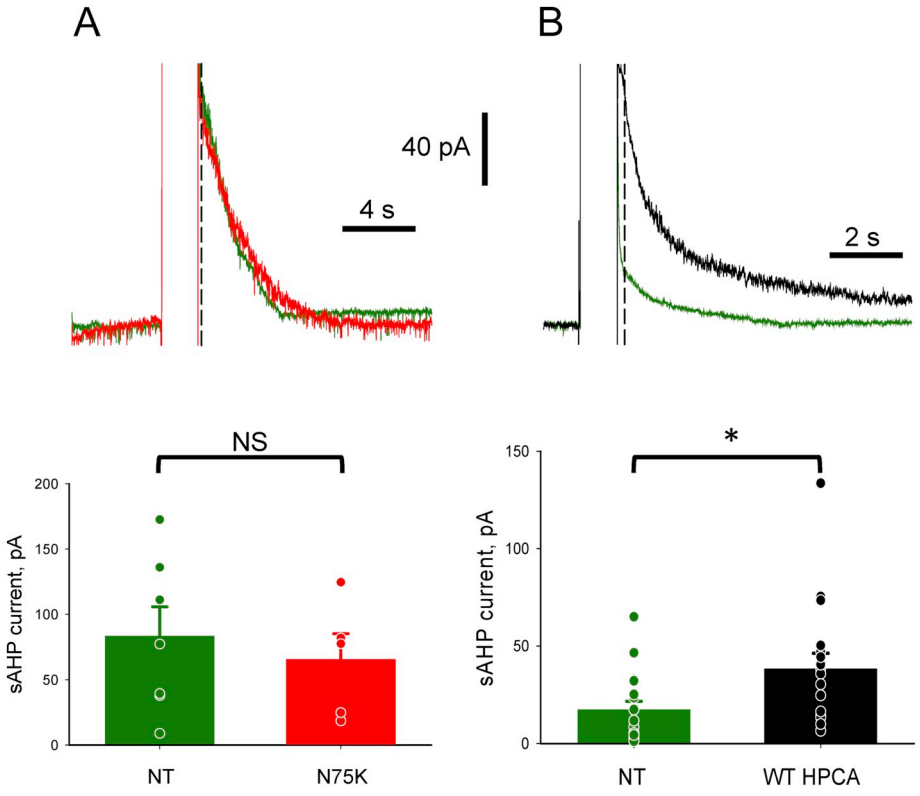

Fig. 6. N75K mutant neither inhibits nor activates sAHP current.
A. Expression of N75K mutant did not affect sAHP current in the hippocampal neurons. Recordings of the currents induced by depolarization pulses (2 s) in non-transfected neurons (green) and neurons expressing N75K mutant (red) (top). Graph summarizing the effect of N75K expression on sAHP current compared to non-transfected neurons as measured by the amplitude of the current (200 ms following the end of the depolarizing pulse (dashed line) to 10 s) (bottom). B. Overexpression of WT HPCA increased sAHP current. Recordings of the currents induced by a depolarization pulse (1 s) in non-transfected neurons (green) and neurons overexpressing WT HPCA (black) (top). Pooled results demonstrating the effect of WT HPCA overexpression compared to one of endogenously expressed HPCA as measured by the amplitude of sAHP current (200 ms following the end of the depolarizing pulse (dashed line) to 10 s) (bottom). (For interpretation of the references to colour in this figure legend, the reader is referred to the web version of this article.)

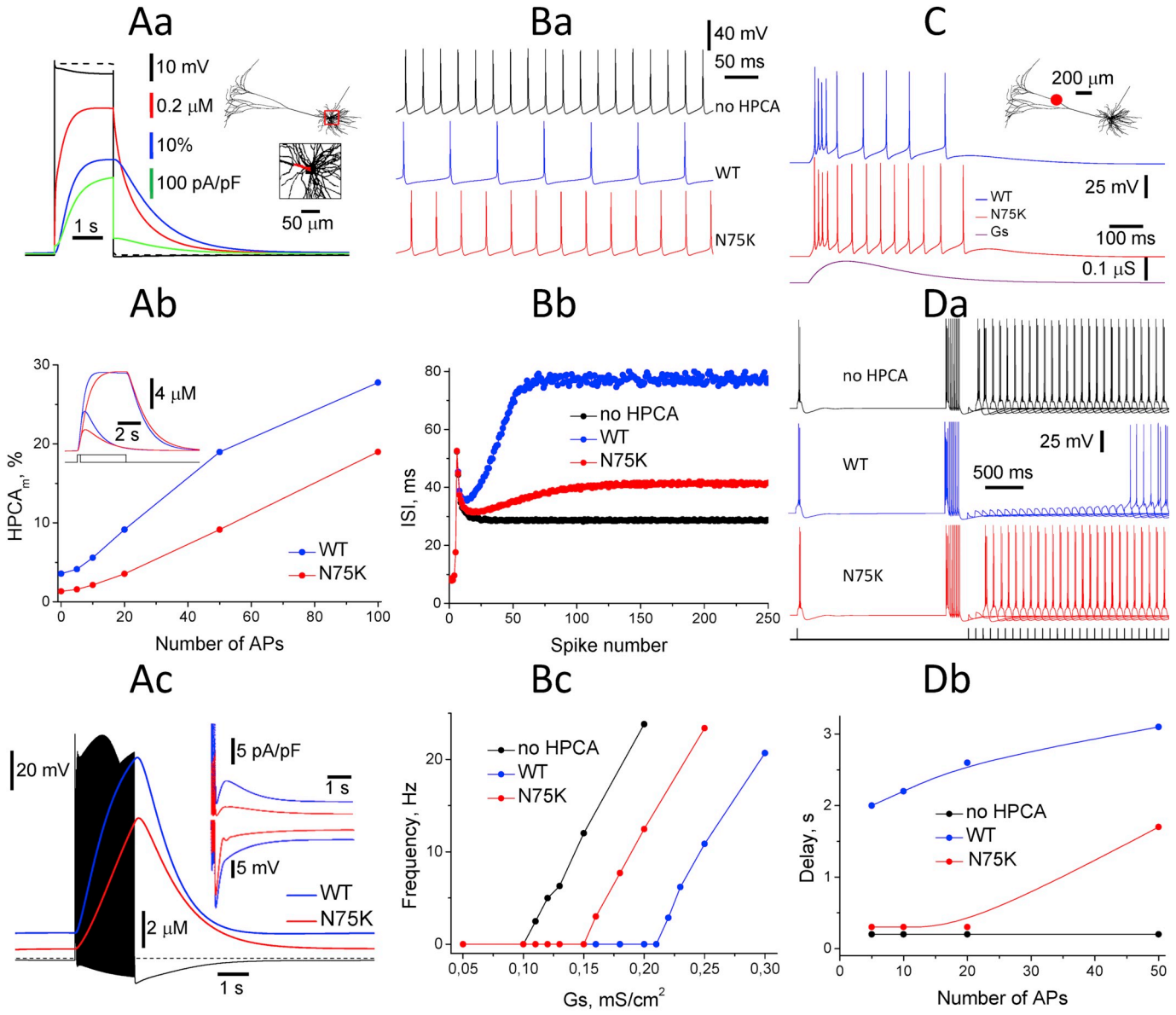

Fig. 7. N75K mutation increases neuronal excitability.

Simulations of changes in excitability induced by N75K mutation were performed using Mainen and Sejnowski model (Mainen and Sejnowski, 1996) of neocortical layer 5 pyramidal neuron developed in the NEURON program environment (Hines and Carnevale, 2001). Aa. Simulation of HPCA translocation and sAHP current induced by depolarization in a voltage clamp mode. Neuronal morphology used for the model is shown in the upper insert. sAHP conductance was gated by HPCA translocated to the plasma membrane of the proximal part of the apical dendrite shown in red in the lower insert. sAHP current (green trace) was activated by somatic depolarization (dashed black trace) inducing depolarization in the proximal dendrite (black trace), increase in $[Ca^{2+}]_i$ (red trace), HPCA translocation to the plasma membrane (blue trace) and gating of sAHP conductance. Colour of scale bars match one of traces. The lower insert depicts with higher magnification a part of the neuron indicated by a red box in the upper insert. Ab. Model parameters describing WT HPCA and N75K interaction with Ca^{2+} and the plasma membrane were fitted to reproduce experimental results obtained in different experimental conditions. A graph demonstrates dependence of HPCA and N75K translocation to the plasma membrane of the proximal dendrite on the number of action potentials generated by a neuron (compare the graph with experimental results shown in Fig. 4D). Y axis represents a proportion of HPCA and its N75K mutant translocated from the cytosol to the plasma membrane. An insert demonstrates both HPCA and N75K mutant translocation transients simulated in response to depolarization of 0.5 s and 4.0 s from −70 to 0 mV (the respective experimental result is present in Fig. 3B). Ac. Simulation of HPCA and N75K translocation and sAHP in response to a train of 100 APs @ 50 Hz in a neuron co-expressing both proteins. An insert shows sAHP currents (upper traces) and sAHP (lower traces) following short (5 APs) trains for a neuron expressing either WT HPCA or N75K mutant. Note a substantial decrease in sAHP current and sAHP for the neuron expressing N75K instead of WT HPCA. Ba-Bc. N75K mutation increases neuronal excitability in response to tonic glutamatergic stimulation. Ba. Simulated neuronal firing induced by the same prolonged (2 s) tonic activation of somatic glutamate receptors leading to conductance of 0.25 mS/cm^2 when (i) HPCA was not introduced into the model (black trace), (ii) HPCA was introduced at concentration of 30 μM (blue trace), and (iii) N75K mutant was introduced at concentration of 30 μM instead of HPCA (red trace). Note substantially higher AP frequency of tonic firing when N75K was introduced in the model instead of WT HPCA. Bb. Inter spike intervals (ISI) are shown for the same cases as in Ba after the tonic receptor activation demonstrating a robust difference in AP adaptation between the models including either WT HPCA and N75K. Bc. Dependence of steady-state frequency of APs on the value of tonic glutamate receptor-induced conductance. Note a wide window in the tonic conductance (0.15–0.21 mS/cm^2), in which tonic firing was observed only in N75K-expressing neurons. C. A transient activation of glutamatergic conductance (bottom trace) evoked a stronger burst of somatic APs in a model with N75K mutant compared to one with WT HPCA demonstrating slower adaptation and higher excitability produced by the mutation. The conductance was located at a red-marked site of the dendritic tree shown in the insert. Da-Db. sAHP, induced by a train of APs decreased an ability of the neuron to reach AP threshold in response to synaptic stimulation. A brief synaptic stimulation evoking a burst of two APs was produced by somatic simulation of glutamatergic conductance. Da. The longest delay in neuronal ability to

generate APs in response to synaptic stimulation after a train of APs inducing sAHP was found for cells expressing the WT HPCA. The delay was many fold shorter for cells expressing N75K mutant instead of WT HPCA, indicating to the increased neuronal excitability induced by this mutation. The synaptic stimulation leading to a short burst (2 APs) was produced at the beginning of each simulation. An induction of 10 back-propagating APs resulted in developing of sAHP and suppression of the burst evoked the synaptic stimulation for 2 s and 0.2 s for the WT HPCA and N75K mutant, respectively. Db. Dependences of the delay in ability to generate the burst after the trains on the number of APs in the trains. The dependences demonstrate a substantial decrease in duration of these intervals in neurons expressing N75K mutant instead of WT HPCA. (For interpretation of the references to colour in this figure legend, the reader is referred to the web version of this article.)

(Figs. 2A, 3A, 4A), although the value and duration of translocation was smaller and shorter, respectively (Figs. 2C, D; 3B–F; 4B–E). We hypothesized that the decreased mutant translocation should lead to a proportional decrease of sAHP if N75K and WT HPCA are equally potent to activate sAHP upon translocation to the plasma membrane (although, an additional decrease of sAHP is likely due to improper mutant signaling in the membrane).

The hippocampal neurons express up to 30 μM of endogenous WT HPCA (Furuta et al., 1999), while the expression level for exogenously expressed proteins hardly exceed 10–15 μM (Cherkas et al., 2018). Thus, the exogenous expression of WT HPCA may result in the increased (up to 50%) amount of HPCA translocated to the plasma membrane (both endogenous and exogenous) and a proportional increase of sAHP. In contrast, N75K mutant, having impaired translocation to the plasma membrane, is unlikely to increase sAHP.

sAHP current was recorded from both N75K transfected and non-transfected cultured hippocampal neurons as an outward tail current developing after cell depolarization (2 s) from −55 to +30 mV (Fig. 6A). This duration of depolarization was chosen to produce fairly large elevations of $[Ca^{2+}]_i$ necessary to induce substantial sAHP current and certain N75K translocation; the latter could potentially contribute to additional activation of sAHP current. Nevertheless, we did not observe an increase in values of sAHP current in N75K transfected compared to non-transfected neurons (Fig. 6A, $p = .9$, $n = 7$ for NT and n = 5 for N75K expressing cells) indicating to incapability of N75K mutant to gate additional sAHP current. The sAHP current was also not significantly inhibited by the translocation suggesting that N75K did not substantially interfere with the endogenous WT HPCA, which gated sAHP.

It is possible that the increase of sAHP current in N75K transfected neurons was not observed since sAHP conductance was fully activated by translocation of endogenous HPCA. In order to test this suggestion, we checked if overexpression of WT HPCA increased the sAHP current. The currents were recorded in non-transfected neurons and in neurons co-transfected with WT HPCA and CFP. We found, that the mean sAHP current amplitude was significantly increased in cells overexpressing the WT HPCA (Fig. 6B, $p < .05$, $n = 17$ for both NT and WT HPCA expressing cells). Thus, expression of exogenous WT HPCA contrary to N75K mutant increased sAHP current.

Altogether, we demonstrated that N75K mutant did not contribute to the gating of sAHP current.

3.7. N75K mutation increases neuronal excitability

Based on our experimental results, we next modeled whether N75K mutation increases neuronal excitability. Simulations were performed on a well-known model of *neocortical layer 5 pyramidal neuron* (Mainen and Sejnowski, 1996) developed in the NEURON program environment (Hines and Carnevale, 2001). sAHP conductance gated by HPCA translocated to the plasma membrane of proximal part of apical dendrite (Power et al., 2011) was included to the model. It was considered in the model that HPCA was subjected to a Ca^{2+}-myristoyl switch after binding of three calcium ions (O'Callaghan et al., 2003; Raghuram et al., 2012) and translocated to the plasma membrane by diffusion (Dovgan et al., 2010; Markova et al., 2008; O'Callaghan et al., 2003). The translocated HPCA gated sAHP conductance according to a first order reaction between HPCA and channels underlying the conductance. It was considered that HPCA translocated to the proximal part of apical dendrite (first 70 μm) (Power et al., 2011) did only contribute to generation of sAHP current (Fig. 7Aa). At high level of $[Ca^{2+}]_i$ both WT HPCA and N75K mutant translocated to the same plasma membrane loci in the proximal part of dendrite (Figs. 3, 4) where the mutant could also potentially gate the potassium conductance. We considered in the model that both proteins are equally capable of controlling sAHP conductance upon their translocation (Fig. 7Ac).

Kinetic constants for interaction of HPCA and N75K mutant with Ca^{2+} and plasma membrane were fitted (Table 1) in order to reproduce amplitudes and decays of translocation transients observed in our experiments (compare Fig. 3B with Fig. 7Aa, Ab insert; Fig. 4B with Fig. 7Ac; Fig. 4D with Fig. 7Ab). The constants relating the sAHP conductance and amount of HPCA translocated to the plasma membrane were further fitted based on measurements of sAHP current (compare Fig. 6 with Fig. 7Aa, Ac).

We modeled several most common conditions leading to neuronal activity in cortical neurons and determined whether an exchange of HPCA for N75K resulted in the increased neuronal excitability. First, we simulated tonic activation of ionotropic receptors (Le Le Meur et al., 2007; Pai et al., 2016; Shen et al., 2017) mediated by a release of astrocyte-derived gliotransmitters (Rose et al., 2017). The tonic activation of somatically located receptors (conductance of 0.25 mS/cm^2) produced a regular high frequency firing of cortical neuron (Fig. 7Ba). Introduction of sAHP conductance gated by HPCA in the model led to a substantial decrease in the frequency of the firing while gating by N75K mutant resulted only in a minor decrease in steady-state firing frequency (Fig. 7Ba). Firing adaptation following the tonic receptor activation was also significantly different in simulations involving HPCA and N75K mutant (Fig. 7Bb). Moreover, HPCA-gated sAHP completely abolished the firing in a wide range of conductance produced by the tonic activation of ionotropic receptors while N75K mutant was substantially less effective (Fig. 7Bc). Altogether, these simulations demonstrate that HPCA signaling is necessary to control the tonic activity of cortical neurons and that N75K mutation results in a significant increase of this activity.

Next, we studied capability of cortical neuron to adaptation in a response to a short synaptic stimulation resembling threshold EPSPs. Fig. 7C, showing an example of such stimulation, demonstrates that both the number of generated APs and inter-spike intervals were substantially modulated by N75K mutation. The mutation resulted in the increased number of APs generated in response to the threshold synaptic stimulation and weaker adaption within the AP burst demonstrating the increased neuronal excitability of cortical neuron.

Trains of back propagating APs in cortical neurons produce the prolonged afterhyperpolarization decreasing neuronal excitability for several seconds in both electrophysiological (Power et al., 2011) and simulation experiments (Fig. 7Da). In a series of simulations, we estimated a time window, in which a dendritic synaptic stimulation evoking a double spike response before the train of 10 back propagating APs was not able to evoke spikes after the burst. This window was very narrow (about 150 ms; black traces in Fig. 7Da) for a model of cortical neuron without sAHP conductance and was mediated by induction of small conductance Ca^{2+}-dependent potassium current included in the model. Incorporation of sAHP conductance gated by HPCA produced a prolonged delay in capability of the neuron to respond to the synaptic stimulation by AP generation (time window of about 2000 ms; blue traces in Fig. 7Da). Besides, first four threshold synaptic stimulations evoked one rather than two APs. When N75K mutant was included in the model instead of HPCA, the threshold responses were resumed after the delay, which was similar to one observed in the model lacking sAHP

conductance (time window of about 200 ms; red traces in Fig. 7Da). Similar results were obtained in our simulations after the AP bursts having a wide range of number of APs (Fig. 7Db). It is interesting to note that the largest difference in the excitability was demonstrated for the burst of 5–10 APs more frequently occurring in the cortical neurons than stronger bursts.

Thus, our simulation experiments indicate that the decreased translocation of N75K mutant to the plasma membrane significantly increases neuronal excitability in many different conditions occurring in the brain.

4. Discussion

Previous studies have demonstrated that point mutations in HPCA causes autosomal-recessive primary isolated dystonia (Charlesworth et al., 2015) and result in abnormal biophysical and functional properties of some HPCA mutants (Helassa et al., 2017). However, molecular and cellular mechanisms relating these point mutations to an aberrant increase in neuronal excitability observed during dystonia (Ibanez et al., 1999; Levy and Hallett, 2002) still remained elusive. Combining molecular genetics with electrophysiology, imaging and modeling, we showed that N75K dystonic HPCA mutant has abnormal Ca^{2+} buffering, impaired Ca^{2+}-dependent signaling and does not control slow afterhyperpolarization normally gated by HPCA translocation to the plasma membrane. This results in the increased neuronal excitability that is likely to underlie manifestation of dystonic symptoms.

4.1. Biophysical properties of N75K mutant

In many cases, disease-causing mutations can affect protein stability or synthesis leading to changes in protein expression levels or preventing the expression itself (Atasu et al., 2018). This was not the case for T71N and N75K HPCA mutations. Our experiments showed that both HPCA mutants had levels of expression similar to one of WT HPCA when exogenously expressed in the same HEK cells and hippocampal neurons (Figs. 1–4). This result is in good agreement with recent data demonstrating that T71N mutation does not affect protein folding, stability and functioning in SH-SY5Y cells (Helassa et al., 2017). Thus, both mutants were expressed in the cells under study and alterations in their signaling, if any, was likely due to the difference in their biophysical properties.

In this work, we have shown that N75K mutant has a lower total Ca^{2+} buffer capacity than WT HPCA in a physiological range of free intracellular calcium concentrations (Fig. 1D–F). Besides, this mutant was also relatively weaker than WT HPCA in binding Ca^{2+} near the basal level of $[Ca^{2+}]_i$ (Fig. 1K) and bound Ca^{2+} relatively stronger in the upper physiological range of $[Ca^{2+}]_i$ (Fig. 1L). Thus, a Ca^{2+}-dependency of buffer capacity of N75K was changed by this mutation. A Ca^{2+}-dependency of T71N Ca^{2+} buffering was also modified compared to WT HPCA although this modification was not as prominent as observed in N75K (Fig. 1L).

N75K and T71N mutations are located within the second EF-hand Ca^{2+}-binding domain of HPCA and are critical to the domain's Ca^{2+}-binding properties. N75K mutation leads to a substitution of the second Ca^{2+}-coordinating residue of the binding sequence within EF-hand 2 domain (Charlesworth et al., 2015). Besides, in this mutation, neutral asparagine is exchanged for a positively charged lysine, which may certainly create an obstacle for binding of the similarly charged calcium ion. Our results strongly suggest that Ca^{2+} is unlikely to be bound by the second EF-hand domain in N75K mutant or its binding is significantly impaired leading to the lower affinity for Ca^{2+}. In both cases the calcium buffer capacity of N75K is decreased compared to WT HPCA and Ca^{2+}-dependency of its buffer capacity is shifted towards higher values of $[Ca^{2+}]_i$.

Although threonine in a position 71 is not an obligatory Ca^{2+} coordinator, T71N mutation is predicted to be damaging, with near maximal probability scores, by all four in silico prediction programs (Charlesworth et al., 2015). Despite prediction, this mutation does not substantially affect the total Ca^{2+} buffering although Ca^{2+}-dependency of the buffering is changed indicating to some minor modification in Ca^{2+}-binding of EF-hand 2 domain of this mutant. These changes are in line with ones observed by Helassa et al. who demonstrated that T71N mutation did not alter the overall calcium-binding affinity but significantly reduced the calcium-binding cooperativity (Helassa et al., 2017).

Hippocalcin plays a significant role as Ca^{2+} buffer in central neurons (Raghuram et al., 2012). High levels of HPCA expression have been reported for cortical and subcortical neurons (Charlesworth et al., 2015; Furuta et al., 1999). On average, HPCA is expressed in the hippocampus at a concentration of 30 μM (Furuta et al., 1999) and its concentration in striatum, an area connected to movement disorders, could be even higher (Charlesworth et al., 2015). Analysis of gene expression patterns of different neuronal Ca^{2+} sensor proteins, to which HPCA belongs, at the cellular level revealed that there is substantial inhomogeneity in the protein expression levels between different cell populations within the same brain regions (Girard et al., 2015). Thus, the very high expression level of HPCA in certain neuronal subpopulations is likely to be achieved. Even at 30 μM, HPCA seems to be the strongest Ca^{2+} buffer at least in the hippocampal neurons (Raghuram et al., 2012). Taking into account that each HPCA molecule can bind calcium ions at EF-hand domain 2, 3 and 4 (Helassa et al., 2017; Raghuram et al., 2012), the total Ca^{2+} buffer capacity of HPCA can be close 100 μM. A high Ca^{2+} affinity of these binding sites (Helassa et al., 2017; O'Callaghan et al., 2003) indicates that HPCA plays a major role in neurons as a Ca^{2+} buffer at a basal level of $[Ca^{2+}]_i$. An impediment to the binding of Ca^{2+} at EF-hand 2 domain of N75K mutant is likely to result in Ca^{2+} binding at the EF-hand 3 domain only, at least at near basal level of $[Ca^{2+}]_i$, thus decreasing Ca^{2+} buffering by HPCA by two-fold (Ames et al., 2002; Li et al., 2011). This powerful downregulation of the major Ca^{2+}-binding protein could severely affect downstream Ca^{2+}-dependent signaling in neurons of descending pathways controlling skeletal muscle contraction. Such changes in Ca^{2+} buffer capacity seem to lead to faster and higher $[Ca^{2+}]_i$ transients in neurons expressing N75K mutants evoked in response to the same Ca^{2+} mobilization into the cytosol. Since HPCA is almost homogeneously distributed in cytosol (Cherkas et al., 2018; Dovgan et al., 2010; Markova et al., 2008), the alterations in Ca^{2+} buffering is likely to result in an abnormal Ca^{2+} signaling in soma, dendrites and axons leading to important physiological consequences that may contribute to manifestations of dystonia. Since HPCA plays a dual role in neuronal regulation as a buffer and sensor, the impaired Ca^{2+} buffering of the N75K mutant is likely to affect its Ca^{2+}-dependent signaling even if its other molecular properties are not modified by this mutation.

In HPCA, binding of Ca^{2+} to functional EF-hand domains operates a Ca^{2+}-myristoyl switch, a conformational transition in the molecule resulting in protrusion of myristoyl group out of a hydrophobic pocket (Ames et al., 1997). The switch controls the ability of HPCA to translocate to target membranes and interact with downstream effectors (Dovgan et al., 2010; O'Callaghan et al., 2003). We found that, in spite of impaired Ca^{2+}-binding at the EF-hand 2 domain, both mutants do translocate to the membranes at high level of $[Ca^{2+}]_i$ demonstrating that the Ca^{2+}-myristoyl switch mechanism is not substantially affected by these mutations. Moreover, high and prolonged elevations of $[Ca^{2+}]_i$ resulted in equal and similarly distributed translocation of both N75K and WT HPCA to the plasma membrane of hippocampal neurons. The results show that not only the Ca^{2+}-myristoyl switch mechanism is preserved in N75K at high levels of $[Ca^{2+}]_i$, but that ability of N75K to be inserted into specific membrane loci is also not affected by this mutation. Previous studies of other similar NCS proteins, revealed that two calcium ions bind sequentially, first at high affinity EF-hand 3 to

facilitate Ca^{2+}-binding at lower affinity EF-hand 2 (Ames et al., 2002; Li et al., 2011) and Ca^{2+}-binding at both sites seems to be necessary for HPCA translocation (O'Callaghan et al., 2003). Thus, it is likely that Ca^{2+} is bound at EF-hand 2 of N75K although at higher $[Ca^{2+}]_i$, than in WT HPCA. Alternatively, the binding of Ca^{2+} to EF-hand 3 only leads to a unclamping of the myristoyl group of N75K, as it has been demonstrated for E85Q recoverin mutant, designed to abolish Ca^{2+} binding to EF-hand 2 (Ames et al., 2002). Whatever maintains the Ca^{2+}-myristoyl switch mechanism functional in N75K at high levels of $[Ca^{2+}]_i$, the more important observation is that the switch is impaired at lower levels of $[Ca^{2+}]_i$ in N75K (compared to WT HPCA), as revealed by robust suppression of its translocation at these conditions (Figs. 2–4). Thus, our findings strongly suggests inability of N75K to bind Ca^{2+} at EF-hand 2 domain, at least at $[Ca^{2+}]_i$ close to its basal level, that abolishes the Ca^{2+}-myristoyl switch normally functioning in WT HPCA in this condition.

4.2. Functional consequences of N75K mutation

In this work we have shown that impaired Ca^{2+} binding at EF-hand 2 domain of N75K prevents decoding of physiologically relevant $[Ca^{2+}]_i$ transients into HPCA translocation to the plasma membrane for activating its membranous targets. Main types of neuronal activity, such as short trains of action potentials (up to 20 APs) and single theta-bursts do not produce substantial N75K translocation to the plasma membrane (Figs. 4,5). Moreover, decoding of trains of theta-bursts by HPCA translocation is also substantially suppressed by N75K mutation (Fig. 5). It is generally accepted that HPCA interaction with the membranes is a necessary step in its transduction mechanism (Andrade et al., 2012; Palmer et al., 2005; Tzingounis et al., 2007). Since N75K mutation prevents Ca^{2+}-dependent HPCA translocation in soma and dendrites of neurons during the main types of neuronal activity, the mutation is likely to result in loss of function of HPCA signaling.

It was initially suggested that HPCA deficiency, induced by T71N and N75K mutations, might downregulate voltage-dependent Ca^{2+} channels, thus far affecting the cellular response to membrane depolarization (Charlesworth et al., 2015). This initial suggestion seems to be supported by recent results also demonstrating abnormal regulation of these channels in cells expressing dystonic mutants of HPCA (Helassa et al., 2017). However, these authors have demonstrated that HPCA oligomerises in Ca^{2+}-dependent manner and binds to voltage-gated calcium channels and that both T71N and A190T mutants showed a defect in oligomerization resulting in an increased Ca^{2+} influx driven by N-type voltage-gated calcium channels (Helassa et al., 2017), thus far directly demonstrating upregulation of Ca^{2+} channels. At the same time, our data indicate that, translocation of the WT HPCA induced by activation of voltage-gated Ca^{2+} channels in the presence (Figs. 3, 4) or absence (Dovgan et al., 2010; Markova et al., 2008) of N75K appear to be similar implying that N75K is unlikely to substantially modulate Ca^{2+} channels in dendrites of the hippocampal neurons. Thus, it seems that different mutations (N75K vs T71N and A190T) introduce differential changes to HPCA signaling with an enhanced $[Ca^{2+}]_i$ signaling observed for T71N and A190T mutants and with the impaired translocation shown here for N75K mutant. Another explanation for this discrepancy is that L-, T-, and R- (Higley and Sabatini, 2008) rather than N-type Ca^{2+} channels contribute to $[Ca^{2+}]_i$ signaling in the neuronal dendrites. Therefore, dendritic $[Ca^{2+}]_i$ signaling is unlikely to be modified by T71N and A190T mutants. We would rather expect to observe an increase in a synaptic vesicle release as a functional consequence of these mutations since N-type Ca^{2+} channels are expressed in the presynaptic terminals where they control a neurotransmitter release (Simms and Zamponi, 2014).

One of the main known functions of HPCA is to gate sAHP after its translocation to the plasma membrane (Tzingounis et al., 2007). We have shown that translocation of N75K to the plasma membrane of neuronal apical dendrite, a part of neuron involved in generation of sAHP current (Power et al., 2011), was significantly suppressed compared to WT HPCA (Figs. 3–5). This suppression was accompanied by inability of N75K to gate additional sAHP current on the top of one gated by endogenous HPCA translocation, while expression of exogenous WT HPCA did increase this current (Fig. 6). Based on these results and previous studies (Andrade et al., 2012; Tzingounis et al., 2007; Villalobos and Andrade, 2010), we have suggested that sAHP conductance is mediated by the first order reaction between HPCA inserted to the membrane and still unknown potassium channel underlying sAHP current. A model of cortical neuron incorporating Ca^{2+}-dependent HPCA signaling and sAHP gating by HPCA fairly reproduces both HPCA translocation and sAHP current observed in our experiments in cells expressing WT HPCA or it N75K mutant (Fig. 7A). Simulations studies based on this model have undoubtedly demonstrated an increased neuronal excitability of cortical neuron expressing N75K instead of WT HPCA. The increase has been demonstrated in conditions reproducing well-known mechanisms of AP generation in central neurons. In particular, we have shown that N75K mutation produces earlier initiation or increased frequency of tonic neuronal activity (Fig. 7B), increased AP generation and impaired adaptation of AP frequency within bursts induced by synaptic stimulation (Fig. 7C) and decreased interburst intervals during repetitive firing (Fig. 7D).

Functional studies suggest that aberrant increased excitability in both cortical and subcortical regions of descending pathways regulating skeletal muscle contraction is a key pathophysiological mechanism of dystonia (Ibanez et al., 1999; Levy and Hallett, 2002). Since HPCA is ubiquitously expressed in neurons of these pathways (Charlesworth et al., 2015; "Hippocalcin expression pattern in cortex GENSAT Project at Rockefeller University, Mouse Brain Atlas, Image Navigator,", 2019; "Hippocalcin expression pattern in spinal cord GENSAT Project at Rockefeller University, Mouse Brain Atlas, Image Navigator,", 2019), the increased neuronal excitability induced by its N75K mutation is likely to be a major cellular mechanism leading to twisting, repetitive movements and abnormal postures observed in dystonic patients.

Although abnormalities of the striatal rather than hippocampal or cortical neurons are considered to be more directly associated with dystonic symptoms, impaired sAHP gating caused by DYT2 mutations of HPCA in these brain regions may contribute to the pathophysiology of DYT2 dystonia. Besides, sAHP, which controls firing patterns in the striatal neurons (Goldberg et al., 2009; Goldberg and Wilson, 2005) expressing HPCA at a particular high level (Charlesworth et al., 2015), seems to be also affected by N75K mutation resulting in the increased excitability of these neurons in DYT2. This suggestion is strongly supported by recent data demonstrating that blocking of channels contributing to sAHP (Tzingounis et al., 2010; Tzingounis and Nicoll, 2008) in substantia nigra pars compacta results in contralateral dystonic posturing (Shi et al., 2013). In addition, sAHP current is also reduced in rat parkinsonism and this reduction increases excitability of striatal cholinergic interneurons (Sanchez et al., 2011). Moreover, sAHP is under strong inhibitory cholinergic control and this inhibition results in the increased neuronal excitability (Ghamari-Langroudi and Bourque, 2004; Klink and Alonso, 1997). Importantly, anticholinergics therapy, which seems to strongly disinhibit sAHP, is an effective symptomatic treatment of dystonic patient (Balint et al., 2018). Interestingly, in mouse models of DYT1 dystonia, an electrophysiological analysis also showed abnormal involvement of different types of AHP (Ponterio et al., 2018; Sciamanna et al., 2011). Altogether, these results indicate that modulation of AHP is likely a common pathway utilized by the nervous system in different pathological conditions. Further research centered on identification of specific populations of striatal neurons with impaired sAHP is certainly warranted for studies of both DYT2 and other movement disorders.

Two homozygous novel truncating mutations in the HPCA gene have been recently revealed in two unrelated Turkish dystonia families presenting with complex dystonia (Atasu et al., 2018). These and Charlesworth et al. (Charlesworth et al., 2015) results together with our

findings imply that any loss of function HPCA mutation is likely to result in development of primary dystonia. Most probably, the development is due to suppression of inhibition in the brain related to decrease or complete loss of sAHP in certain neuronal populations. Recently, an acceleration of the spontaneous pacemaker frequency and reduction in sAHP associated with dysregulation of HPCA ubiquitination have been shown for noradrenergic neurons in mouse Parkinson's disease model (Key et al., 2019). Additionally, studies on Huntington disease (Luthi-Carter et al., 2002; Luthi-Carter et al., 2000) show a great reduction of HPCA mRNA in the striatal neurons coincidental with onset of dystonic symptoms in Huntington mouse model. This evidence also supports the idea that abnormal HPCA signaling leads to a dysregulation of movement control. Thus, further genetic screening of patients having primary dystonia or other neurological movement disorders for mutations and/or abnormal expression of *HPCA* and *Neurocalcin δ*, genes encoding proteins involved in gating of sAHP (Villalobos and Andrade, 2010), is warranted to expose both a genetic cause and molecular and cellular mechanisms of these disorders.

Interestingly, HPCA KO mice, being impaired on a discrimination learning task, revealed no significant abnormalities in motor activity (Kobayashi et al., 2005). Most probably, other genes of neuronal Ca^{2+} sensor family (Burgoyne et al., 2019) compensated for *HPCA* in KO mice while N75K mutation in humans, being only partially nonfunctional according to this work, did not resulted in such a compensation (Rossi et al., 2015). The other reason for the normal motor activity of HPCA KO mice is substantial distinctions of their brain and spinal circuits involved in movement control compared to humans. N75K KI mice, which might be a perfect animal model of DYT2, are required to understand the lack of abnormalities in motor activity of HPCA KO mice.

Our results strongly suggest that genetic interventions leading to the increased expression of the WT HPCA in abnormally excited descending pathways regulating skeletal muscles would restore slow afterhyperpolarization in neurons of these pathways and would be an effective tool to treat patients with DYT2 dystonia.

In conclusion, we have shown that N75K mutant, contrary to the WT HPCA, cannot translocate to the plasma membrane of dendritic compartments in response to physiologically relevant patterns of neuronal activity. This impairment renders the mutant incapable of controlling slow afterhyperpolarization and, consequently, increases neuronal excitability likely underlying primary dystonia.

Declaration of Competing Interest

Authors declare no conflict of interest.

Acknowledgements

This work was funded by the National Academy of Sciences of Ukraine (NASU) (grants #0116U004470 and #67/15 to PB) and Osteopathic Heritage Foundation (grant #67260 to VV).

References

Ames, J.B., Ishima, R., Tanaka, T., Gordon, J.I., Stryer, L., Ikura, M., 1997. Molecular mechanics of calcium-myristoyl switches. Nature 389, 198–202. https://doi.org/10.1038/38310.

Ames, J.B., Hamasaki, N., Molchanova, T., 2002. Structure and calcium-binding studies of a recoverin mutant (E85Q) in an allosteric intermediate state. Biochemistry 41, 5776–5787.

Andrade, R., Foehring, R.C., Tzingounis, A.V., 2012. The calcium-activated slow AHP: cutting through the Gordian knot. Front. Cell. Neurosci. 6, 47. https://doi.org/10.3389/fncel.2012.00047.

Atasu, B., Hanagasi, H., Bilgic, B., Pak, M., Erginel-Unaltuna, N., Hauser, A.K., Guven, G., Simón-Sánchez, J., Heutink, P., Gasser, T., Lohmann, E., 2018. HPCA confirmed as a genetic cause of DYT2-like dystonia phenotype. Mov. Disord. 33, 1354–1358. https://doi.org/10.1002/mds.27442.

Balint, B., Mencacci, N.E., Valente, E.M., Pisani, A., Rothwell, J., Jankovic, J., Vidailhet, M., Bhatia, K.P., 2018. Dystonia. Nat. Rev. Dis. Prim. 4, 25. https://doi.org/10.1038/s41572-018-0023-6.

Belan, P., Kostyuk, P., Snitsarev, V., Tepikin, A., 1993. Calcium clamp in isolated neurones of the snail Helix pomatia. J. Physiol. 462, 47–58.

Bostan, A., Strick, P.L., 2012. The cerebellum and basal ganglia are interconnected. Neuropsychol. Rev. 20, 261–270. https://doi.org/10.1007/s11065-010-9143-9.The.

Burgoyne, R.D., Helassa, N., Mccue, H.V., Haynes, L.P., 2019. Calcium sensors in neuronal function and dysfunction. Cold Spring Harb. Perspect. Biol., a035154. https://doi.org/10.1101/cshperspect.a035154.

Byun, K., Kim, D., Bayarsaikhan, E., Oh, J., Kim, J., Kwak, G., Jeong, G.-B., Jo, S.-M., Lee, B., 2013. Changes of calcium binding proteins, c-Fos and COX in hippocampal formation and cerebellum of Niemann–pick, type C mouse. J. Chem. Neuroanat. 52, 1–8. https://doi.org/10.1016/j.jchemneu.2013.04.006.

Ceballos-Baumann, A.O., Brooks, D.J., 1997. Basal ganglia function and dysfunction revealed by PET activation studies. Adv. Neurol. 74, 127–139.

Ceballos-Baumann, A.O., Passingham, R.E., Warner, T., Playford, E.D., Marsden, C.D., Brooks, D.J., 1995. Overactive prefrontal and underactive motor cortical areas in idiopathic dystonia. Ann. Neurol. 37, 363–372. https://doi.org/10.1002/ana.410370313.

Charlesworth, G., Angelova, P.R., Bartolomé-Robledo, F., Ryten, M., Trabzuni, D., Stamelou, M., Abramov, A.Y., Bhatia, K.P., Wood, N.W., 2015. Mutations in HPCA cause autosomal-recessive primary isolated dystonia. Am. J. Hum. Genet. 96, 657–665. https://doi.org/10.1016/j.ajhg.2015.02.007.

Cherkas, V., Grebenyuk, S., Osypenko, D., Dovgan, A.V., Grushevskyi, E.O., Yedutenko, M., Sheremet, Y., Dromaretsky, A., Bozhenko, A., Agashkov, K., Kononenko, N.I., Belan, P., 2018. Measurement of intracellular concentration of fluorescently-labeled targets in living cells. PLoS One 13, e0194031. https://doi.org/10.1371/journal.pone.0194031.

Dovgan, A.V., Cherkas, V.P., Stepanyuk, A.R., Fitzgerald, D.J., Haynes, L.P., Tepikin, A.V., Burgoyne, R.D., Belan, P.V., 2010. Decoding glutamate receptor activation by the Ca2+ sensor protein hippocalcin in rat hippocampal neurons. Eur. J. Neurosci. 32, 347–358. https://doi.org/10.1111/j.1460-9568.2010.07303.x.

Edwards, M.J., Huang, Y.Z., Wood, N.W., Rothwell, J.C., Bhatia, K.P., 2003. Different patterns of electrophysiological deficits in manifesting and non-manifesting carriers of the DYT1 gene mutation. Brain 126, 2074–2080. https://doi.org/10.1093/brain/awg209.

Faas, G.C., Mody, I., 2012. Measuring the kinetics of calcium binding proteins with flash photolysis. Biochim. Biophys. Acta 1820, 1195–1204. https://doi.org/10.1016/j.bbagen.2011.09.012.

Fierro, L., Llano, I., 1996. High endogenous calcium buffering in Purkinje cells from rat cerebellar slices. J. Physiol. 496 (Pt 3), 617–625.

Foehring, R.C., Zhang, X.F., Lee, J.C.F., Callaway, J.C., 2009. Endogenous calcium buffering capacity of substantia nigral dopamine neurons. J. Neurophysiol. 102, 2326–2333. https://doi.org/10.1152/jn.00038.2009.

Furuta, Y., Kobayashi, M., Masaki, T., Takamatsu, K., 1999. Age-related changes in expression of hippocalcin and NVP2 in rat brain. Neurochem. Res. 24, 651–658.

Ghamari-Langroudi, M., Bourque, C.W., 2004. Muscarinic receptor modulation of slow afterhyperpolarization and phasic firing in rat supraoptic nucleus neurons. J. Neurosci. 24, 7718–7726. https://doi.org/10.1523/JNEUROSCI.1240-04.2004.

Girard, F., Venail, J., Schwaller, B., Celio, M.R., 2015. The EF-hand Ca(2+)-binding protein super-family: a genome-wide analysis of gene expression patterns in the adult mouse brain. Neuroscience 294, 116–155. https://doi.org/10.1016/j.neuroscience.2015.02.018.

Goldberg, J.A., Wilson, C.J., 2005. Control of spontaneous firing patterns by the selective coupling of calcium currents to calcium-activated potassium currents in striatal cholinergic interneurons. J. Neurosci. 25, 10230–10238. https://doi.org/10.1523/JNEUROSCI.2734-05.2005.

Goldberg, J. a, Teagarden, M. a, Foehring, R.C., Wilson, C.J., 2009. Nonequilibrium calcium dynamics regulate the autonomous firing pattern of rat striatal cholinergic interneurons. J. Neurosci. 29, 8396–8407. https://doi.org/10.1523/JNEUROSCI.5582-08.2009.

Helassa, N., Antonyuk, S.V., Lian, L.Y., Haynes, L.P., Burgoyne, R.D., 2017. Biophysical and functional characterization of hippocalcin mutants responsible for human dystonia. Hum. Mol. Genet. 26, 2426–2435. https://doi.org/10.1093/hmg/ddx133.

Helmchen, F., Imoto, K., Sakmann, B., 1996. Ca2+ buffering and action potential-evoked Ca2+ signaling in dendrites of pyramidal neurons. Biophys. J. 70, 1069–1081. https://doi.org/10.1016/S0006-3495(96)79653-4.

Higley, M.J., Sabatini, B.L., 2008. Calcium signaling in dendrites and spines: practical and functional considerations. Neuron 59, 902–913. https://doi.org/10.1016/j.neuron.2008.08.020.

Hines, M.L., Carnevale, N.T., 2001. NEURON: A Tool for Neuroscientists. vol. 7. Neurosci, pp. 123–135.

Hines, M.L., Morse, T., Migliore, M., Carnevale, N.T., Shepherd, G.M., 2004. ModelDB: a database to support computational neuroscience. J. Comput. Neurosci. 17, 7–11. https://doi.org/10.1023/B:JCNS.0000023869.22017.2e.

Hippocalcin expression pattern in cortex GENSAT Project at Rockefeller University, 2019. Mouse Brain Atlas, Image Navigator. WWW Document. http://gensat.org/imagenavigator.jsp?imageID=26722 (accessed 2.2.17).

Hippocalcin expression pattern in spinal cord GENSAT Project at Rockefeller University, 2019. Mouse Brain Atlas, Image Navigator. WWW Document. http://gensat.org/imagenavigator.jsp?imageID=26137 (accessed 2.2.17).

Ibanez, V., Sadato, N., Karp, B., Deiber, M.-P., Hallett, M., 1999. Deficient activation of the motor cortical network in patients with writer's cramp. Neurology 53, 96–105. https://doi.org/10.1212/WNL.53.1.96.

Iwabuchi, S., Kakazu, Y., Koh, J.-Y., Harata, N.C., 2013. Abnormal cytoplasmic calcium dynamics in central neurons of a dystonia mouse model. Neurosci. Lett. 548, 61–66. https://doi.org/10.1016/j.neulet.2013.05.047.

Kakazu, Y., Koh, J.-Y., Iwabuchi, S., Gonzalez-Alegre, P., Harata, N.C., 2012. Miniature release events of glutamate from hippocampal neurons are influenced by the dystonia-associated protein torsinA. Synapse 66, 807–822. https://doi.org/10.1002/syn.21571.

Key, J., Mueller, A.K., Gispert, S., Matschke, L., Wittig, I., Corti, O., Münch, C., Decher, N., Auburger, G., 2019. Ubiquitylome profiling of Parkin-null brain reveals dysregulation of calcium homeostasis factors ATP1A2, Hippocalcin and GNA11, reflected by altered firing of noradrenergic neurons. Neurobiol. Dis. 127, 114–130. https://doi.org/10.1016/j.nbd.2019.02.008.

Kim, K.S., Kobayashi, M., Takamatsu, K., Tzingounis, A.V., 2012. Hippocalcin and KCNQ channels contribute to the kinetics of the slow afterhyperpolarization. Biophys. J. 103, 2446–2454. https://doi.org/10.1016/j.bpj.2012.11.002.

Klink, R., Alonso, A., 1997. Muscarinic modulation of the oscillatory and repetitive firing properties of entorhinal cortex layer II neurons. J. Neurophysiol. 77, 1813–1828.

Kobayashi, M., Takamatsu, K., Saitoh, S., Noguchi, T., 1993. Myristoylation of hippocalcin is linked to its calcium-dependent membrane association properties. J. Biol. Chem. 268, 18898–18904.

Kobayashi, M., Masaki, T., Hori, K., Masuo, Y., Miyamoto, M., Tsubokawa, H., Noguchi, H., Nomura, M., Takamatsu, K., 2005. Hippocalcin-deficient mice display a defect in cAMP response element-binding protein activation associated with impaired spatial and associative memory. Neuroscience 133, 471–484. https://doi.org/10.1016/j.neuroscience.2005.02.034.

Kuba, R., Tyrlíková, I., Brázdil, M., Rektor, I., 2010. Lateralized ictal dystonia of upper and lower limbs in patients with temporal lobe epilepsy. Epileptic Disord. 12, 109–115. https://doi.org/10.1684/epd.2010.0310.

Larson, J., Munkácsy, E., 2015. Theta-burst LTP. Brain Res. 1621, 38–50. https://doi.org/10.1016/j.brainres.2014.10.034.

Lee, S.H., Rosenmund, C., Schwaller, B., Neher, E., 2000. Differences in Ca2+ buffering properties between excitatory and inhibitory hippocampal neurons from the rat. J. Physiol. 525 (Pt 2), 405–418.

Levy, L.M., Hallett, M., 2002. Impaired brain GABA in focal dystonia. Ann. Neurol. 51, 93–101. https://doi.org/10.1002/ana.10073.

Li, C., Pan, W., Braunewell, K.H., Ames, J.B., 2011. Structural analysis of Mg2+ and Ca2+ binding, myristoylation, and dimerization of the neuronal calcium sensor and visinin-like protein 1 (VILIP-1). J. Biol. Chem. 286, 6354–6366. https://doi.org/10.1074/jbc.M110.173724.

Luthi-Carter, R., Strand, A., Peters, N.L., Solano, S.M., Hollingsworth, Z.R., Menon, A.S., Frey, A.S., Spektor, B.S., Penney, E.B., Schilling, G., Ross, C.A., Borchelt, D.R., Tapscott, S.J., Young, A.B., Cha, J.H., Olson, J.M., 2000. Decreased expression of striatal signaling genes in a mouse model of Huntington's disease. Hum. Mol. Genet. 9, 1259–1271. https://doi.org/10.1093/hmg/9.9.1259.

Luthi-Carter, R., Hanson, S.A., Strand, A.D., Bergstrom, D.A., Chun, W., Peters, N.L., Woods, A.M., Chan, E.Y., Kooperberg, C., Krainc, D., Young, A.B., Tapscott, S.J., Olson, J.M., 2002. Dysregulation of gene expression in the R6/2 model of polyglutamine disease: parallel changes in muscle and brain. Hum. Mol. Genet. 11, 1911–1926. https://doi.org/10.1093/hmg/11.17.1911.

Madison, D.V., Nicoll, R.A., 1984. Control of the repetitive discharge of rat CA 1 pyramidal neurones in vitro. J. Physiol. 354, 319–331.

Mainen, Z.F., Sejnowski, T.J., 1996. Influence of dendritic structure on firing pattern in model neocortical neurons. Nature 382, 363–366. https://doi.org/10.1038/382363a0.

Markova, O., Fitzgerald, D., Stepanyuk, A., Dovgan, A., Cherkas, V., Tepikin, A., Burgoyne, R.D., Belan, P., 2008. Hippocalcin signaling via site-specific translocation in hippocampal neurons. Neurosci. Lett. 442, 152–157. https://doi.org/10.1016/j.neulet.2008.06.089.

Le Meur, K., Galante, M., Angulo, M.C., Audinat, E., 2007. Tonic activation of NMDA receptors by ambient glutamate of non-synaptic origin in the rat hippocampus. J. Physiol. 580, 373–383. https://doi.org/10.1113/jphysiol.2006.123570.

Migliore, M., Morse, T.M., Davison, A.P., Marenco, L., Shepherd, G.M., Hines, M.L., 2003. ModelDB: making models publicly accessible to support computational neuroscience. Neuroinformatics 1, 135–139. https://doi.org/10.1385/NI:1:1:135.

Neher, E., Augustine, G.J., 1992. Calcium gradients and buffers in bovine chromaffin cells. J. Physiol. 450, 273–301.

O'Callaghan, D.W., Ivings, L., Weiss, J.L., Ashby, M.C., Tepikin, A.V., Burgoyne, R.D., 2002. Differential use of myristoyl groups on neuronal calcium sensor proteins as a determinant of spatio-temporal aspects of Ca 2+ signal transduction. J. Biol. Chem. 277, 14227–14237. https://doi.org/10.1074/jbc.M111750200.

O'Callaghan, D.W., Tepikin, A.V., Burgoyne, R.D., 2003. Dynamics and calcium sensitivity of the Ca2+/myristoyl switch protein hippocalcin in living cells. J. Cell Biol. 163, 715–721. https://doi.org/10.1083/jcb.200306042.

Pai, Y.H., Lim, C.S., Park, K.-A., Cho, H.S., Lee, G.-S., Shin, Y.S., Kim, H.-W., Jeon, B.H., Yoon, S.H., Park, J.B., 2016. Facilitation of AMPA receptor-mediated steady-state current by extrasynaptic NMDA receptors in supraoptic magnocellular neurosecretory cells. Korean J. Physiol. Pharmacol. 20, 425–432. https://doi.org/10.4196/kjpp.2016.20.4.425.

Palmer, C.L., Lim, W., Hastie, P.G.R., Toward, M., Korolchuk, V.I., Burbidge, S.a., Banting, G., Collingridge, G.L., Isaac, J.T.R., Henley, J.M., 2005. Hippocalcin functions as a calcium sensor in hippocampal LTD. Neuron 47, 487–494. https://doi.org/10.1016/j.neuron.2005.06.014.

Papoutsi, A., Kastellakis, G., Poirazi, P., 2017. Basal tree complexity shapes functional pathways in the prefrontal cortex. J. Neurophysiol. 118, 1970–1983. https://doi.org/10.1152/jn.00099.2017.

Parrilla-Carrero, J., Buchta, W.C., Goswamee, P., Culver, O., Mckendrick, G., Harlan, B., Moutal, A., Penrod, R., Lauer, A., Ramakrishnan, V., Khanna, R., Kalivas, P., Riegel, A.C., 2018. Restoration of Kv7 channel-mediated inhibition reduces cued-reinstatement of cocaine seeking. J. Neurosci. 38, 4212–4229. https://doi.org/10.1523/JNEUROSCI.2767-17.2018.

Piccinin, C.C., Piovesana, L.G., Santos, M.C., Guimarães, R.P., De Campos, B.M., Rezende, T.J., Campos, L.S., Torres, F.R., Amato-Filho, A.C., França Jr., M.C., Lopes-Cendes, I., Cendes, F., D'Abreu, A., 2015. Diffuse decreased gray matter in patients with idiopathic craniocervical dystonia: a voxel-based morphometry study. Front. Neurol. 5, 283. https://doi.org/10.3389/fneur.2014.00283.

Ponterio, G., Tassone, A., Sciamanna, G., Vanni, V., Meringolo, M., Santoro, M., Mercuri, N.B., Bonsi, P., Pisani, A., 2018. Enhanced mu opioid receptor–dependent opioidergic modulation of striatal cholinergic transmission in DYT1 dystonia. Mov. Disord. 33, 310–320. https://doi.org/10.1002/mds.27212.

Power, J.M., Bocklisch, C., Curby, P., Sah, P., 2011. Location and function of the slow afterhyperpolarization channels in the basolateral amygdala. J. Neurosci. 31, 526–537. https://doi.org/10.1523/JNEUROSCI.1045-10.2011.

Raghuram, V., Sharma, Y., Kreutz, M.R., 2012. Ca(2+) sensor proteins in dendritic spines: a race for Ca(2+). Front. Mol. Neurosci. 5, 61. https://doi.org/10.3389/fnmol.2012.00061.

Rasouli, L., Rasouli, J.J., Panov, F., Yoo, J.Y., Mcgoldrick, P.E., Frucht, S., Wolf, S., Ghatan, S., 2018. Simultaneous treatment of epilepsy and secondary dystonia after anterior temporal lobectomy and amygdalohippocampectomy. World Neurosurg. 117, 439–442. https://doi.org/10.1016/j.wneu.2018.04.003.

Rose, C.R., Felix, L., Zeug, A., Dietrich, D., Reiner, A., Henneberger, C., 2017. Astroglial glutamate signaling and uptake in the hippocampus. Front. Mol. Neurosci. 10, 451. https://doi.org/10.3389/fnmol.2017.00451.

Rossi, A., Kontarakis, Z., Gerri, C., Nolte, H., Hölper, S., Krüger, M., Stainier, D.Y.R., 2015. Genetic compensation induced by deleterious mutations but not gene knockdowns. Nature 524, 230–233. https://doi.org/10.1038/nature14580.

Sabatini, B.L., Oertner, T.G., Svoboda, K., 2002. The life cycle of Ca(2+) ions in dendritic spines. Neuron 33, 439–452.

Sanchez, G., Rodriguez, M.J., Pomata, P., Rela, L., Murer, M.G., 2011. Reduction of an afterhyperpolarization current increases excitability in striatal cholinergic interneurons in rat parkinsonism. J. Neurosci. 31, 6553–6564. https://doi.org/10.1523/JNEUROSCI.6345-10.2011.

Sciamanna, G., Tassone, A., Martella, G., Mandolesi, G., Puglisi, F., Cuomo, D., Madeo, G., Ponterio, G., Standaert, D.G., Bonsi, P., Pisani, A., 2011. Developmental profile of the aberrant dopamine D2 receptor response in striatal cholinergic interneurons in DYT1 dystonia. PLoS One 6, e24261. https://doi.org/10.1371/journal.pone.0024261.

Shen, W., Nikolic, L., Meunier, C., Pfrieger, F., Audinat, E., 2017. An autocrine purinergic signaling controls astrocyte-induced neuronal excitation. Sci. Rep. 7, 11280. https://doi.org/10.1038/s41598-017-11793-x.

Shi, L., Bian, X., Qu, Z., Ma, Z., Zhou, Y., Wang, K., Jiang, H., Xie, J., 2013. Peptide hormone ghrelin enhances neuronal excitability by inhibition of Kv7/KCNQ channels. Nat. Commun. 4, 1435. https://doi.org/10.1038/ncomms2439.

Simms, B.A., Zamponi, G.W., 2014. Neuronal voltage-gated calcium channels: structure, function, and dysfunction. Neuron 82, 24–45. https://doi.org/10.1016/j.neuron.2014.03.016.

Smit, M., Vállez García, D., de Jong, B.M., Zoons, E., Booij, J., Dierckx, R.A., Willemsen, A.T., de Vries, E.F., Bartels, A.L., Tijssen, M.A., 2018. Relationships between serotonin transporter binding in the raphe nuclei, basal ganglia, and hippocampus with clinical symptoms in cervical dystonia: a [11C]DASB positron emission tomography study. Front. Neurol. 9, 88. https://doi.org/10.3389/fneur.2018.00088.

Tanabe, L.M., Kim, C.E., Alagem, N., Dauer, W.T., 2009. Primary dystonia: molecules and mechanisms. Nat. Rev. Neurol. 5, 598–609. https://doi.org/10.1038/nrneurol.2009.160.

Tomic, A., Agosta, F., Sarasso, E., Petrovic, I., Basaia, S., Pesic, D., Kostic, M., Fontana, A., Kostic, V.S., Filippi, M., 2018. Are there two different forms of functional dystonia? A multimodal brain structural MRI study. Mol. Psychiatry. https://doi.org/10.1038/s41380-018-0222-2.

Tzingounis, A.V., Nicoll, R. a, 2008. Contribution of KCNQ2 and KCNQ3 to the medium and slow afterhyperpolarization currents. Proc. Natl. Acad. Sci. U. S. A. 105, 19974–19979. https://doi.org/10.1073/pnas.0810535105.

Tzingounis, A.V., Kobayashi, M., Takamatsu, K., Nicoll, R.A., 2007. Hippocalcin gates the calcium activation of the slow afterhyperpolarization in hippocampal pyramidal cells. Neuron 53, 487–493. https://doi.org/10.1016/j.neuron.2007.01.011.

Tzingounis, A.V., Heidenreich, M., Kharkovets, T., Spitzmaul, G., Jensen, H.S., Nicoll, R. a, Jentsch, T.J., 2010. The KCNQ5 potassium channel mediates a component of the afterhyperpolarization current in mouse hippocampus. Proc. Natl. Acad. Sci. U. S. A. 107, 10232–10237. https://doi.org/10.1073/pnas.1004644107.

Villalobos, C., Andrade, R., 2010. Visinin-like neuronal calcium sensor proteins regulate the slow calcium-activated afterhyperpolarizing current in the rat cerebral cortex. J. Neurosci. 30, 14361–14365. https://doi.org/10.1523/JNEUROSCI.3440-10.2010.

Vitko, I., Chen, Y., Arias, J.M., Shen, Y., Wu, X.-R., Perez-Reyes, E., 2005. Functional characterization and neuronal modeling of the effects of childhood absence epilepsy variants of CACNA1H, a T-type calcium channel. J. Neurosci. 25, 4844–4855. https://doi.org/10.1523/JNEUROSCI.0847-05.2005.

Widman, A.J., Stewart, A.E., Erb, E.M., Gardner, E., Mcmahon, L.L., 2018. Intravascular ketamine increases theta-burst but not high frequency tetanus induced LTP at CA3-CA1 synapses within three hours and devoid of an increase in spine density. Front. Synaptic Neurosci. 10, 8. https://doi.org/10.3389/fnsyn.2018.00008.

Yokoi, F., Chen, H.-X., Dang, M.T., Cheetham, C.C., Campbell, S.L., Roper, S.N., Sweatt, J.D., Li, Y., 2015. Behavioral and electrophysiological characterization of Dyt1 heterozygous knockout mice. PLoS One 10, e0120916. https://doi.org/10.1371/journal.pone.0120916.